Theory of high-field electron transport in silicon dioxide

M. V. Fischetti, D. J. DiMaria, S. D. Brorson,* T. N. Theis, and J. R. Kirtley
IBM Thomas J. Watson Research Center, Yorktown Heights, New York 10598
(Received 8 February 1985)

A Monte Carlo technique is employed to simulate the electron transport in SiO_2 at high electric fields (from 1.5×10^6 to 12×10^6 V/cm). Both the polar and the nonpolar electron-phonon scattering processes are considered. We show that the nonpolar interaction with the acoustic and band-edge phonons is a mechanism which must be included in order to explain the experimental evidence of a steady-state electron-transport regime at high average electron energy ($\simeq$3—4 eV) at these high fields. The LO phonons alone cannot prevent the electrons from running away at fields above 2×10^6 V/cm, while at higher fields the main effect of the nonpolar scattering is that of randomizing the electron momenta via large-angle scattering, thus stabilizing the electron-energy distributions. The average energies and the energy relaxation distances obtained from the Monte Carlo simulation agree very well with the experimental data, particularly when collisional broadening effects are introduced in the simulation. Internal photoemission of electrons from an aluminum or a silicon electrode into SiO_2 is also simulated, and the results agree with the well-known data indicating an effective relaxation length of about 3 nm for electrons in SiO_2. Comparison is also made between the experimental and theoretical electron-energy distributions at high fields ($\gtrsim 8\times10^6$ V/cm). The results indicate that at very high electron energies the band structure of SiO_2 and quantum transport effects may reduce the effective scattering rates. While the semiclassical Monte Carlo solution seems to be reasonably valid for electron energies up to about 4 eV, more sophisticated approaches are needed to investigate the high-energy tails of the electron distributions.

I. INTRODUCTION

Silicon dioxide is the most commonly employed insulator in the solid-state industry. Since very-large-scale-integration (VLSI) technology requires smaller devices with thinner insulating films, it is of crucial importance to understand the properties of the amorphous SiO_2 films subject to high electric fields. Dramatic device failures, due to effects, such as, threshold-voltage shifts in field-effect transistors or dielectric breakdown, are probably related to the high flow of energetic electrons in the SiO_2 conduction band. Carriers are injected into the insulator after having gained large amounts of energy in the active semiconducting regions of the device and may also tunnel into the SiO_2 if sufficiently high fields are applied across the insulating layers. Thus, the understanding of the mechanisms which lead to the degradation and breakdown of the devices is strictly dependent on the understanding of the mechanism of transport and energy loss of electrons in the SiO_2.

Some authors have already reported a series of experiments showing that electrons in the SiO_2 conduction band can easily gain more energy than predicted by the theoretical picture developed in the past decade, which is based only on the polar electron-phonon scattering.[1–3] Recently, Fischetti has also shown, by a Monte Carlo simulation, that the new experimental observations can be understood if proper account is made also for the nonpolar electron-acoustic phonon scattering.[4] The scope of this paper is to briefly review the problem of the electron transport in amorphous SiO_2 at high electric fields ($\gtrsim 10^6$ V/cm) in the light of the new data, and to present in more detail the approximations employed and the results of the Monte Carlo simulation performed in Ref. 4.

This paper is organized as follows: In Sec. II we review the problem of high-field electron transport in silicon dioxide. In Sec. III we consider the electron-phonon scattering rates appropriate to SiO_2 and in Sec. IV we discuss the difficulties with the semiclassical approach employed to solve the transport problem. In Sec. V, the Monte Carlo technique we have used and its implementation are discussed. Section VI presents the significant results of the simulation and, finally, in Sec. VII, we draw a few conclusions.

II. PROBLEM OF HOT ELECTRONS IN SiO_2

A. Electron transport in ionic insulators

The problem of electron transport in ionic insulators, such as the alkali halides, has been tackled several times in the past 50 years.[5–8] In these materials the strong interaction between the electrons and the polar molecules of the dielectric has been assumed to be the only significant mechanism of electron-energy loss, with the exception only of Refs. 7 and 8. This mechanism is very effective for electron energies comparable to the energy of the longitudinal-optical (LO) phonons of the insulator. However, at sufficiently high electron velocities, the lattice can no longer follow the motion of the electrons and the rate at which the electrons lose their energy in polarizing the lattice decreases as the electron energy increases. There exists a critical field, F_{th}, above which most of the electrons gain more energy from the electric field than they

can lose to the lattice polarization waves. In this situation, usually referred to as "velocity runaway," the electron energy increases without limit to the maximum applied voltage; that is, there is no steady-state solution of the electron-transport equation. This is considered to be the threshold of dielectric breakdown,[5–8] since the very energetic electrons can now impact ionize the molecular bonds via inverse Auger scattering, thus causing an avalanche multiplication process which would eventually disrupt the lattice.

B. Standard picture for SiO_2

A similar picture was viewed also for silicon dioxide. Although somewhat less polar than the alkali halides, SiO_2 exhibits two LO-phonon modes (of energies 0.063 and 0.153 eV) which are coupled rather strongly to the conduction electrons.[9] This interaction was believed to be sufficiently strong to maintain a steady-state transport situation up to fields of the order of 10^7 V/cm (Refs. 9 and 10). In the steady-state regime the average electron energies were expected to be of the order of the dominant LO-phonon ($\lesssim$0.15 eV). This implied very short mean free paths ($\sim$0.2 nm) for the electrons at all fields below the runaway threshold. Above this critical field, the electrons could be slowed down only by high-energy processes, such as interband impact ionization, as is the case for the alkali halides. However, rather than a conventional avalanche multiplication breakdown, the generation of electron-hole pairs was suggested to trigger the breakdown process in a different way.[11,12] Due to the low mobility of holes in amorphous SiO_2 (Ref. 13), a positive space charge would result from the steady-state balance between the generation of holes and their recombination with the injected electrons. In turn, this would produce an enhancement of the field at the injecting electrode. Thus, an even higher electron current and faster production of impact-ionized holes would result, and so on in a divergent feedback process which, once more, would somehow cause the destructive breakdown of the dielectric. We shall refer to this model based on LO-phonon scattering *only* (and impact ionization as the breakdown-triggering process) as the "standard model."

The validity of this picture seemed to be confirmed by several additional results, both experimental and theoretical. First, the electron mobility was measured at *low fields* ($\lesssim 10^6$ V/cm) by Hughes[14] and found to be in agreement with the theoretical expectation based on LO-phonon scattering.[9] Second, during high-field ($\gtrsim 7\times10^6$ V/cm) electron injection via Fowler-Nordheim tunneling into the SiO_2, a buildup of positive charge was observed to occur in the oxide, as predicted by the standard model.[15] Finally, theoretical calculations based on LO-phonon scattering predicted the critical runaway field F_{th} to be in the range of 7×10^6 to 10^7 V/cm (Refs. 9 and 10); that is, in the range of breakdown fields observed experimentally in the middle 70's.

C. Problems with the standard model

The standard model was never unanimously accepted, since some experimental observations seemed to be in sharp contrast with it. Some of the experimental observations which seemed to be in contrast with the standard model are as follows.

(1) *The electron mean free path predicted by the standard model at high fields seemed to be too small* to explain the results of internal photoemission experiments performed in metal-oxide-semiconductor (MOS) structures.[16] The experimental photoyield at a given field and photon energy could be explained only by assuming an "effective scattering length" of about 3 nm in the image-force-lowered barrier between the injecting electrode and the oxide. More recently, resonant tunneling was observed during high-field Fowler-Nordheim injection in thin ($\sim$4.5 nm) SiO_2 (Ref. 17). In order for these resonances to be observed, the electron wave functions must preserve their coherence over distances of about 1.5 to 2.5 nm in the SiO_2 conduction band at fields of about 9×10^6 V/cm. This would not be possible if the electron mean free path for collisions with the LO phonons at these high fields were of the order of 0.2 nm.

(2) *The electron energies seem to be significantly higher than the LO-phonon energy at fields lower than the runaway threshold.* This was deduced from early measurements of the energy of the electrons emitted from the SiO_2 into vacuum.[18] A significant number of electrons was collected at fields of about 8×10^6 V/cm. Since only electrons with energy higher than the SiO_2 work function (0.9 eV) can be collected, a significant number of electrons with energy higher than 0.9 eV are present in SiO_2 at these fields. On the contrary, the standard model predicts that an insignificant number of electrons hotter than 0.15 eV should exist at fields lower than the breakdown field. The same conclusion could be drawn from the sharp drop in the electronic capture cross section for positively charged Coulombic centers in SiO_2 at fields larger than $1-2\times10^6$ V/cm (Ref. 19). This drop could be well accounted for by a significant electron heating much below the runaway threshold.

(3) *The breakdown fields observed at present are much larger than those predicted by the standard model.* We have remarked above that the breakdown fields observed 10 years ago were of the order of 8×10^6 to 10^7 V/cm, as predicted by the ionization-recombination model. Recently, these breakdown fields have increased to the range 1.5×10^7 to 1.8×10^7 V/cm (Ref. 20). Moreover, the anode fields at breakdown do not seem to depend strongly on the oxide thickness, at least in the range of 3 to 50 nm (Ref. 2), contrary to predictions of the standard model. Therefore, it seems that the maximum field strength the insulator can survive is still a function of technological variables, rather than of intrinsic physical processes. As technology improves, higher and higher breakdown fields are obtained and the correlation observed in the past between the field at which velocity runaway occurs, as predicted by the standard model, and the breakdown field seems now to be, at best, merely coincidental.

(4) *Positive charge is formed at high fields in thin SiO_2 even when the total applied voltage is below threshold for impact ionization.*[2,21] Thus, another mechanism must be invoked for the generation of this positive charge and its existence in thicker oxides cannot be claimed to be a manifest proof that impact ionization occurs.

D. Need for a new scattering mechanism

The most serious difficulty with the standard model concerns the average electron energies; that is, item (2) above. In the LO-phonon based picture, the only way electrons can gain energies higher than 0.15 eV is by running away. Indeed, according to the standard model, in the range of energies between the LO-phonon energy and the *lowest* possible threshold for interband impact ionization ($\approx$ the SiO_2 band gap $=9$ eV), there is no other mechanism for energy loss. The presence of electrons with energies significantly higher than 0.15 eV at fields below the velocity runaway threshold cannot be reconciled with this model.

Recently, some of us have shown that significant electron heating occurs already at 3×10^6 V/cm (Refs. 1–3). Three different experimental techniques have been employed. Figures 1–3 illustrate schematically the structures employed and the quantities measured in the three experiments. The first one, called for brevity "electroluminescence," indirectly allows the determination of the average energy of the electrons as they exit the SiO_2 layer of MOS structures and enter the metal gate.[1] These electrons lose energy by exciting surface plasmons at the metal-vacuum interface. In intentionally roughened structures, the coupling between surface plasmons and photons is greatly enhanced and a measurable luminescence is observed.[1,22] From the spectrum of the emitted photons it is possible to derive the average energy of the electrons entering the gate. The second experimental technique ("carrier separation") allows the indirect measurement of the energy of the electrons transported at high fields from the gate to the silicon substrate of p-channel field-effect transistors as they enter the substrate and generate electron-hole pairs in the silicon.[2] Holes and electrons can be independently counted by measuring the currents at the source and/or drain and substrate contacts, respectively. The hotter the electrons, the larger the number of pairs which are generated. Thus, a measurement of the ratio between the hole and electron currents allows the determination of the average energy of the electrons as they exit the oxide. The last technique employed ("vacuum emission") provides direct information about both the average energy and energy distribution of the electrons injected into the SiO_2 from the Si substrate as they travel through the insulator and a thin metal gate and are collected by an analyzing system in a vacuum chamber.[3]

Each technique has advantages and disadvantages. In particular, the interpretation of the data obtained from the photon spectrum in the electroluminescence experiment requires a significant deconvolution and extrapolation. The vacuum emission data may be affected by the electron scattering in the thin metal gate, which may modify the details of the electron-energy distributions. More accurate information is expected from the carrier separation data. In this case, the connection between the average electron energy and the number of electron-hole pairs which are generated in the silicon substrate involves only a deconvolution of the data with the probabilities for a multiple-ionization process in silicon as a function of electron energy. These probabilities have been accurately evaluated and compared with the theoretical model of Alig *et al.*[23]

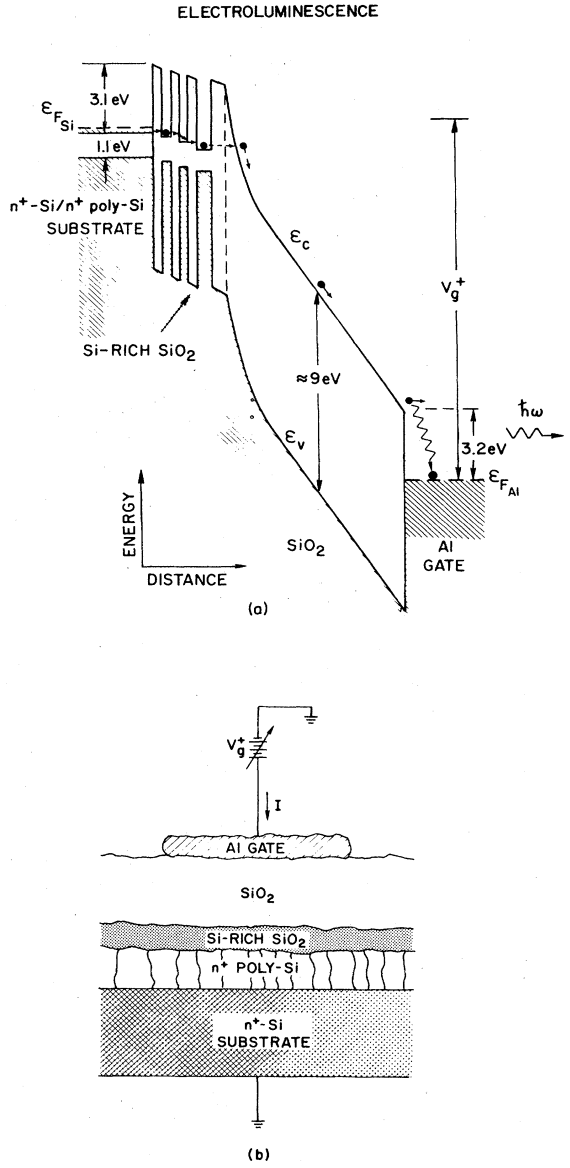

FIG. 1. Schematic band diagram (a) and device structure (b) illustrating the electroluminescence experiment described in Ref. 1. Electrons are injected from the silicon substrate of metal-oxide-silicon capacitors into the SiO_2 layer by using a silicon-rich injector. This avoids premature dielectric breakdown of the insulator. A fraction of the injected electrons lose energy in the metal gate by emitting surface plasmons at the metal-vacuum interface. The plasmons then decay radiatively and the average energy of the electrode is deduced from the spectrum of the emitted photons.

While the details of the picture emerging from these different experiments could be somewhat affected by the interpretation of the data, the main conclusion is remarkably consistent. *The average electron energies, no matter how measured, are significantly higher than the LO-phonon energy even at the lowest fields at which the experi-*

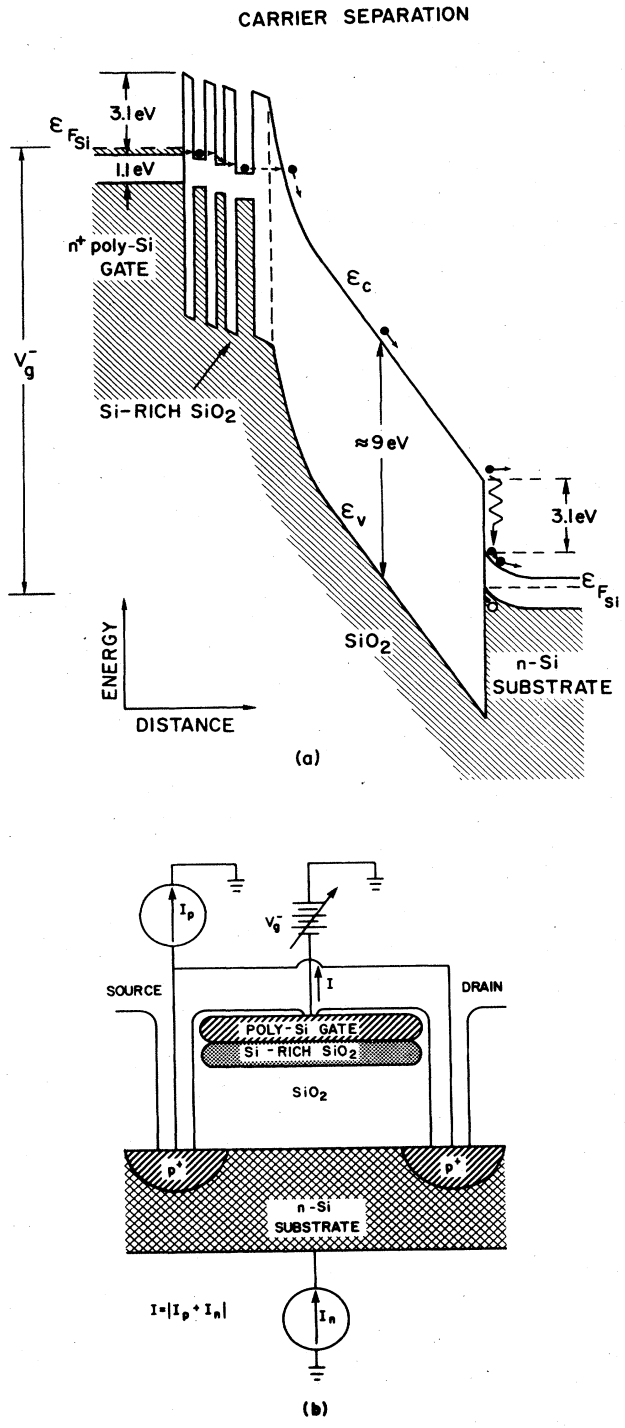

FIG. 2. In the carrier separation experiment described in Ref. 2 the electrons are injected from the polysilicon gate of a *p*-channel field-effect transistor into the silicon substrate. The number of electron-hole pairs generated by the hot electrons as they enter the substrate is obtained by measuring the hole current at the source and/or drain electrodes and the electron current at the substrate contact. The average energy of the carriers is then evaluated by using the known probability for impact ionization in Si as a function of the electron energy.

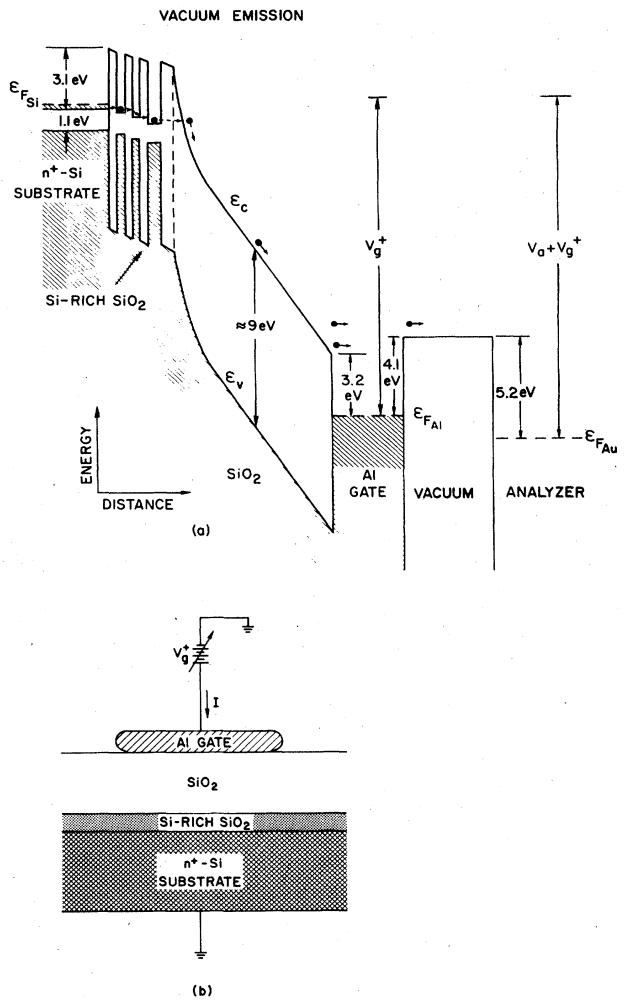

FIG. 3. Band diagram (a) and device structure (b) employed in the vacuum-emission experiment described in Ref. 3. The injected electrons travel through a thin ($\lesssim$25-nm) metal gate and their energy distribution is measured by collecting the carriers with a counting electrode in a vacuum chamber in the presence of a variable retarding potential.

ments were performed ($\sim 3\times 10^6$ V/cm). As shown in Fig. 4, the three techniques indicate that the average electron energy increases almost linearly with the anode field, ranging from about 2 eV at 3.5×10^6 V/cm to about 4 to 5 eV at 10^7 V/cm. No runaway is observed at any field, as the average electron energies do not depend on the SiO_2 thickness in the range 6.6 to 150 nm. Even the energy distributions seem to be only moderately affected by the thickness of the insulator in the range 50 to 150 nm. The distance the electrons must travel in the SiO_2 conduction band before reaching a steady-state regime was found to be of the order of 3 nm, as determined by the dependence of the average energies on SiO_2 thickness in very thin oxide layers. (It follows that the electron energies are almost completely determined by the electric field in the last 3 nm of the insulator they must travel before entering the anode. Therefore, the anode field has been used in Fig. 4.)

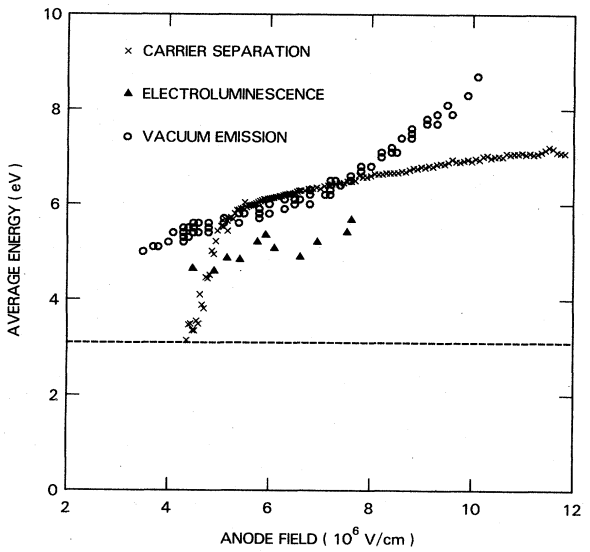

FIG. 4. The average energies of electrons injected into 50-nm-thick SiO_2 layers at different anode fields as obtained from the three techniques of Figs. 1–3. The energies are measured from the bottom of the conduction band of Si (carrier separation) or from the Fermi level of the Al electrode (electroluminescence and vacuum emission). The dashed line indicates the position of the bottom of the SiO_2 conduction band relative to the Al Fermi level or the bottom of the Si conduction band.

This characteristic distance can also be related to the slope of the data in Fig. 4. The average electron energy $\langle w \rangle$ can be expressed as a linear function of the applied anode field with slope:

$$\frac{d\langle w \rangle}{dF_{\text{anode}}} = e\lambda \,, \tag{1}$$

where e is the magnitude of the electron charge and λ (~ 3 nm) is the "energy-relaxation distance" usually employed in the linearized Boltzmann equation.[24]

To complete the picture, it should be noted that the significant heating observed at these low fields *is actually consistent with the LO-phonon scattering.* Indeed, Fitting and Frieman have performed a Monte Carlo simulation of the electron transport in SiO_2 including the Fröhlich scattering with the two dominant LO phonons.[25] Contrary to the results of Lynch[9] and Ferry,[10] they found that velocity runaway should occur already at about 2×10^6 V/cm. We observe that a qualitatively similar conclusion can be reached from the path-integral approach of Thornber and Feynman.[6] As also noted by Lynch, a simple extrapolation of their results to SiO_2 would provide a critical field of 3×10^6 to 4×10^6 V/cm, depending on the choice of the electron effective mass. The following question remains: why did the calculation of Refs. 9 and 10 provide results which are in contrast with the Monte Carlo simulations of Fitting and Frieman and with the experimental observations? Possibly, Lynch's calculations are affected by an overestimation of the energy losses to the LO phonons. His approach, originally due to Fermi,[26] correctly describes the energy losses of heavy and fast particles whose deflection after a collision can be neglected. These undeflected charged particles interact with the electrostatic field of the harmonically bound scatters for longer times, thus losing more energy than light particles, such as electrons in a solid, which have a nonnegligible probability of suffering large-angle scattering. Finally, Ferry seems to obtain solutions of the Boltzmann equation which at high fields ($\gtrsim 7\times10^6$ V/cm) are stable (i.e., the electrons do not runaway) for times probably too short ($\lesssim 10^{-15}$ sec) to apply to realistic injection experiments.

The recent experimental and theoretical results we have outlined in this section clearly indicate that *the LO-phonons cannot prevent the electrons from running away at fields as low as 2×10^6 V/cm. Another scattering mechanism, previously neglected, must be effective at higher fields and energies, to control the steady-state electron transport.*

Acoustic phonons have been already invoked by Sparks *et al.*[8] in the context of avalanche breakdown in alkali halides and they have been shown to be a necessary ingredient to understand the high-field electron transport in these insulators. Ridley[27] has also suggested that in SiO_2 the acoustic phonons may become significant scatterers at high fields and that they may constitute that missing energy-loss mechanism in the "no-loss" energy range between the LO-phonon energy and the threshold for interband impact ionization. Finally, Fischetti has reconsidered this idea and, following the approximations employed by Sparks *et al.* with the appropriate modifications, has implemented it in a semiclassical Monte Carlo simulation.[4] It was concluded that indeed the inclusion of the electron-acoustic phonon scattering can account for the recent experimental results outlined above. In the following, we shall consider these calculations in detail.

III. ELECTRON-PHONON INTERACTION AND THE TRANSPORT PROBLEM

Among the various scattering mechanisms controlling the transport of electrons in a solid, we have considered only the electron-phonon interaction. The electron-electron scattering is negligible because of the very low concentration of carriers (typically much less than 10^{13} electrons/cm^3) present in the SiO_2 conduction band during a Fowler-Nordheim tunnel injection or a photoinjection experiment. Scattering from charged impurities or defects may be significant, in principle. However, on one hand, it is very difficult to know the exact spatial distribution of these ionized centers in the oxide. On the other hand, it has been observed experimentally that the average electron energy is independent of the concentration of negative charges trapped in the bulk oxide (due to filled water-related electron traps) or of positively charged sites at the interface.[2] Therefore, Coulomb scattering with charged centers in the SiO_2 has been neglected. Finally, high-energy processes, such as, interband impact ionization or bulk-plasmon emission, could alter significantly only the high-energy tail of the electron distribution. While this tail may be important in controlling the degradation and breakdown characteristics of the oxide, in this paper we shall restrict our attention to the gross features

of the electron transport and ignore the high-energy collisions.

Electrons can interact with the lattice via polar scattering with optical phonons and via nonpolar scattering with both acoustic and optical phonons. The latter is usually dominant in covalent solids, the former in ionic crystals. SiO_2 has a mixed bonding character,[28] so that both interactions should be considered. As stated above, the inclusion of the nonpolar electron-phonon interaction constitutes the main difference between our calculation and the previous ones. We shall now review the two types of interaction and consider their scattering rates, as usually derived in the literature.[29]

A. Polar electron-phonon interaction

An electron traveling in a polar insulator will interact with the optical phonons via the polarization field of the ions. This interaction is particularly strong in the case of longitudinal phonons, which are associated with a large field, while the transverse-optical phonons are usually ignored. The Hamiltonian describing this Coulombic interaction has been given by Fröhlich in the form:[5,29]

$$H_{\text{polar}}=\sum_{\mathbf{k},\mathbf{q}}\frac{ieG}{q}c^{\dagger}_{\mathbf{k}+\mathbf{q}}c_{\mathbf{k}}(b_{\mathbf{q}}-b^{\dagger}_{-\mathbf{q}}) , \tag{2}$$

where $\mathbf{k}$ and $\mathbf{q}$ are the electron and phonon wave vectors, respectively, $c_{\mathbf{k}}$ and $b_{\mathbf{q}}$ are the electron and phonon operators, and the coupling constant G is given by

$$G^2=\frac{\hbar\omega_{\text{LO}}}{4}\left[\frac{1}{\epsilon_{>}}-\frac{1}{\epsilon_{<}}\right] , \tag{3}$$

where $\epsilon_{>}$ and $\epsilon_{<}$ are the permittivity at frequencies larger and smaller than the optical-phonon frequency ω_{LO}. Since the LO-phonon spectrum mostly presents narrow bands, the dispersion of ω_{LO} is usually ignored.

The magnitude of the phonon momentum q appearing in the denominator of Eq. (2) expresses the Coulombic nature of the interaction. The physical implications relevant to the problem of the electron transport are twofold. First, small momentum-transfer interactions are largely favored in the polar electron-phonon scattering. Thus, the electrons will be largely deflected in the forward direction; that is, in the direction of the field. Second, as the electron energy increases, the effect of the widening of the volume in phase space available to the final states is small, since collisions with short-wavelength phonons are less probable, so that the scattering probability decreases as the electron-energy increases. This typically Coulombic effect is one of the major characteristics of the polar electron-phonon interaction and constitutes the basis of the standard model outlined in Sec. II.

The first-order scattering rate $1/\tau^{(\pm)}_{\text{polar}}$ at finite temperature for emission or absorption of one phonon can be obtained from Eq. (2) by the Fermi rule and by using the effective-mass approximation with parabolic and spherical bands:

$$\frac{1}{\tau^{(\pm)}_{\text{polar}}(\mathbf{k})}=\frac{m^*e^2\omega_{\text{LO}}}{4\pi\hbar^2k}\left[\frac{1}{\epsilon_{>}}-\frac{1}{\epsilon_{<}}\right](n_{\text{LO}}+\tfrac{1}{2}\pm\tfrac{1}{2})\int_{q_{\min}}^{q_{\max}}dq\frac{1}{q} , \tag{4}$$

where m^* is the electron effective mass, $\hbar$ is the Planck's constant divided by 2π, and n_{LO} is the thermally-averaged occupation number of the optical phonons. The upper (lower) sign refers to phonon emission (absorption) and the maximum and minimum momentum transfer allowed by energy-momentum conservation are

$$q_{\max}=\frac{(2m^*)^{1/2}}{\hbar}[w^{1/2}+(w\mp\hbar\omega_{\text{LO}})^{1/2}] ,$$

$$q_{\min}=\pm\frac{(2m^*)^{1/2}}{\hbar}[w^{1/2}-(w\mp\hbar\omega_{\text{LO}})^{1/2}] .$$

where w is the electron energy. Integrating Eq. (4), the scattering rate for emission or absorption of one LO phonon by an electron with energy w is

$$\frac{1}{\tau^{(\pm)}_{\text{polar}}(w)}=\left[\frac{m^*}{2}\right]^{1/2}\frac{e^2\omega_{\text{LO}}}{4\pi\hbar}\left[\frac{1}{\epsilon_{>}}-\frac{1}{\epsilon_{<}}\right]\frac{1}{w^{1/2}}(n_{\text{LO}}+\tfrac{1}{2}\pm\tfrac{1}{2})\times\ln\left[\frac{1+(1\mp\hbar\omega_{\text{LO}}/w)^{1/2}}{\pm1\mp(1\mp\hbar\omega_{\text{LO}}/w)^{1/2}}\right] . \tag{5}$$

B. Nonpolar electron-phonon interaction

Electrons can interact with both acoustic and optical phonons via nonpolar processes in which the electron Bloch waves are perturbed by the displacement of the ions from their equilibrium position. In general, the Hamiltonian describing this kind of interaction can be put in the form:[29]

$$H_{\text{nonpolar}}=\sum_{\mathbf{k},\mathbf{q}}\frac{i\hbar^{1/2}S_{\mathbf{q}}}{(2\rho\omega_{\mathbf{q}})^{1/2}}c^{\dagger}_{\mathbf{k}+\mathbf{q}}c_{\mathbf{k}}(a_{\mathbf{q}}-a^{\dagger}_{-\mathbf{q}}) , \tag{6}$$

ρ being the density of the lattice, $a_{\mathbf{q}}$ is the acoustic- or optical-phonon operator, $\omega_{\mathbf{q}}$ is the phonon frequency and $S_{\mathbf{q}}$ is a coupling constant.

In the case of scattering with acoustic phonons, the strength of the interaction is usually taken to be proportional to the *relative* displacement of the ions from one unit cell to another, and thus proportional to the magnitude of the phonon wave vector q. Indeed, in the limit of a long-wavelength deformation of the lattice, this can be viewed as being uniformly translated over a large region. Therefore, the Bloch waves will be minimally perturbed and the interaction will vanish in the limit $q\rightarrow0$. On the contrary, short-wavelength phonons represent large distorsions of the ionic potential from the equilibrium situation as we move from one cell to another, and the traveling electrons will feel a strong perturbation. In the limit $q\rightarrow0$, Bardeen and Shockley have written the coupling

constant S_q as[30]

$$S_q = C_1 q \tag{7}$$

in the simple case of spherical bands. The factor C_1 is the "deformation potential" and it expresses the variation of the electron energy at the bottom of the conduction band as the linear dimensions of a unit cell are modified by a unit length. In the opposite limit (high phonon momentum), the coupling constant S_q can be expressed in terms of the differential scattering cross section σ_q related to the form factor of the lattice:[29]

$$|S_q|^2 = \frac{\pi\hbar^4 N^2 q^2}{m^{*2}}\sigma_q , \tag{8}$$

where N is the atomic density.

In both limits ($q \to 0$ and $q \to q_{BZ}$, the wave vector at the Brillouin-zone edge), the coupling constant S_q is proportional to the phonon momentum. Thus, the nonpolar interaction with the acoustic phonons exhibits a behavior opposite to the one exhibited by the polar interaction: large-angle scattering is favored with respect to forward scattering—particularly when umklapp processes begin to play a role—and the scattering rate increases with electron energy. Thus, one might expect than this interaction will become dominant at high energies, as was suggested by Ridley.[27]

The nonpolar scattering with optical phonons has been taken by Harrison to be proportional to the *absolute* ion displacement.[31] The energy factor S_q is then the deformation potential, independent of q. Therefore, the nonpolar electron-optical-phonon scattering increases with energy at a slower rate.

For spherical, parabolic bands, Sparks *et al.*[8] have given the expressions for the nonpolar scattering rates in the two limits of low electron energy ($w \ll w_{BZ}$, the electron energy at the edge of the first Brillouin zone), when umklapp processes cannot occur, and in the opposite limit of high electron energies ($w \gg w_{BZ}/2$), when umklapp processes are significant. In the first limit, the rate for emission (for w larger than the cutoff energy $w_c = 2m^* c_s^2$, c_s being the sound velocity) or absorption of a transverse (TA) or longitudinal acoustic (LA) phonon can be written as

$$\frac{1}{\tau^{(\pm)}_{\text{nonpolar}}(w)} = \frac{m^* C_1^2}{4\pi\rho\hbar^2 c_s k}\int_0^{q_{\max}} dq\, q^2 (n_q + \tfrac{1}{2} \pm \tfrac{1}{2}) , \tag{9}$$

where n_q is the thermally averaged acoustic-phonon occupation number. The phonon dispersion relation has been approximated by $\omega_q \simeq \hbar c_s q$. The maximum phonon wave vector which can be emitted or absorbed is $q_{\max} = 2k \mp 2m^* c_s/\hbar$.

Since Eq. (9) is only valid for small electron energies, we can employ a high-temperature expansion of the Bose factor n_q and obtain the usual "deformation-potential" expression for the scattering rate for emission and absorption:[30]

$$\frac{1}{\tau^{(\pm)}_{\text{nonpolar}}(w)} \simeq \frac{3m^{*3/2} C_1^2 k_B T}{2^{1/2}\pi\rho c_s^2 \hbar^4} w^{1/2} , \tag{10}$$

the factor 3 accounting for the three branches (LA and TA) of the acoustic-phonon spectrum, which we consider equivalent.

In the limit of high electron energy, following Sparks *et al.*,[8] we shall assume that an equivalent scattering rate with the band-edge photons can be obtained by substituting in Eq. (9) the lattice density with $M_> / a_0^3$, a_0 being the lattice constant and $M_>$ the mass of the heaviest constituent of the unit cell. Furthermore, the phonon dispersion relation for the transverse and longitudinal modes at the edge of the first Brillouin zone will be approximated by $\omega_{\text{edge}} \approx \hbar c_s q_{BZ}$. Thus, summing over the transverse and longitudinal modes and using Eq. (8), one has

$$\frac{1}{\tau^{(\pm)}_{\text{nonpolar}}(w)} \simeq \frac{8\pi^3\hbar^2 N^2 \sigma}{m^* M_> \omega_{\text{edge}}}\left[\frac{w}{w_{BZ}}\right]^{3/2}(n_{q_{BZ}} + \tfrac{1}{2} \pm \tfrac{1}{2}) , \tag{11}$$

having neglected the dependence of σ on $\mathbf{q}$.

Sparks *et al.* have already shown that the high-energy umklapp processes included in Eq. (11) play a key role in understanding the high-field properties of ionic insulators. The strong energy dependence of the nonpolar electron-phonon interaction is a key issue also in SiO_2, as will be shown.

C. Electron-phonon scattering rates in SiO_2

The scattering rates given by Eqs. (10) and (11) are obtained in the effective-mass approximation, using parabolic and spherical bands. From pseudopotential calculations of the band structure of α quartz,[32] this approximation should be satisfactory for electrons with energy below 1 eV, assuming an effective mass of $0.5 m_{\text{free}}$. At higher electron energies, we have to face several problems. Some of them originate from the questionable validity of the semiclassical solution of the transport problem at high scattering rates, as we discuss in the next section. More problems arise from our poor knowledge of the band structure and density of states for SiO_2. Finally, the amorphous structure of thermally grown SiO_2 poses questions of fundamental nature, such as the definition of umklapp processes, unit cells, or even phonon modes and electron momenta. We ignore this last class of problems, on the heuristic grounds that actually α quartz and thermally grown silicon dioxide exhibit striking similarities in optical and mechanical properties. Thus, α quartz can be employed as a prototype to perform the simulations.

The inadequacy of the available experimental and theoretical data about the detailed structure of the SiO_2 conduction band(s) is a serious issue. From the calculation of Ref. 32 relative to α quartz, we may expect that at electron energies approaching the edge of the first Brillouin zone ($\simeq$5 eV), the density of states may go through a minimum, as the first conduction band terminates. This will probably yield smaller scattering rates than those calculated above. Again, we assume parabolic bands at all electron energies with $m^* \simeq m_{\text{free}}$ and ignore the possibility of intervalley scattering at high energy. Thus, the nonpolar electron-phonon interaction—which controls the electron-energy losses at these high energies—is probably

overestimated. Consistently, we calculate the electron energy at the Brillouin-zone edge, w_{BZ}, by considering a spherical Brillouin zone with volume equal to the volume of the zone in α quartz,[33] obtaining $w_{BZ} \simeq 5.5$ eV. This is consistent with the band structure calculated by Chelikowsky and Schlüter.[32]

Neither the SiO_2 deformation potential, C_1, nor its form factor, S_q, are known. Therefore, the form factor has been estimated from Eq. (8) by assuming that the cross section σ is dominated by the larger oxygen ions. Their integrated cross section, 3.5×10^{-15} cm^2 (from the discussion of Ref. 8), has been rescaled by the average, dynamic effective mass of oxygen in SiO_2 ($\simeq 1.1e$, as given by Pantelides and Harrison[34]), to account for the covalence of the Si—O bond in SiO_2. Thus, from Eq. (10), $|S_q|/q \simeq 3.5$ eV. At low electron energy, the deformation potential should be used to evaluate S_q. However, since the polar interaction controls the transport at low energies, the same coupling constant can be used for the nonpolar scattering at all energies without significant errors. The difference between longitudinal- and transverse-acoustic and band-edge modes has been ignored and an equivalent sound velocity has been obtained by appropriate averaging the longitudinal (c_L) and transverse (c_T) sound velocities: $3/c_s \simeq 2/c_T + 1/c_L$ (Ref. 35).

Finally, the low- and high-energy expressions given by Eqs. (10) and (11), respectively, have been algebraically interpolated between $w_{BZ}/2$ and w_{BZ}. Different interpolations have been employed (either requiring simply the continuity of the scattering rates or also the continuity of higher-order derivatives) without obtaining appreciable differences in the final results.

Figure 5 shows the scattering rates obtained from the approximations discussed. Both LO-phonon modes are included to evaluate the polar scattering rate. The coupling constants for these interactions have been taken from Lynch[9] ($\epsilon_0/\epsilon_> - \epsilon_0/\epsilon_< \simeq 0.063$ and 0.143 for the low- and high-energy polar modes, respectively, ϵ_0 being the vacuum permittivity). The nonpolar scattering is with LA and TA phonons at low energy and with the band-edge phonons at high energy. The low-energy nonpolar interaction between electrons and optical phonons is neglected, since it is not expected to contribute appreciably when a reasonable choice ($\approx 10^8$ eV/cm) is made for the deformation potential.

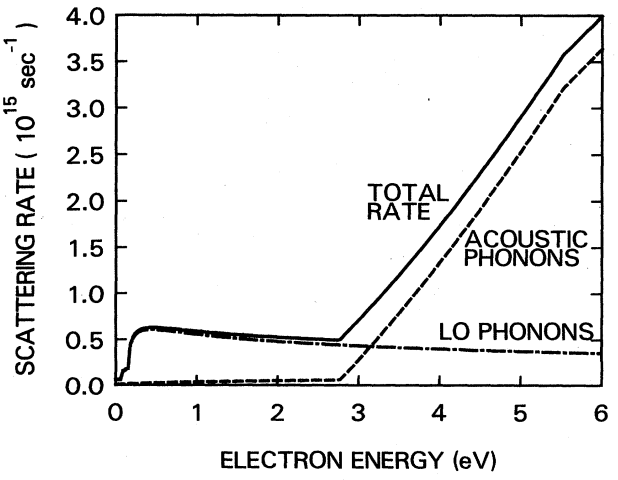

FIG. 5. Polar, nonpolar, and total electron-phonon scattering rates in SiO_2 at 298 K when collisional-broadening effects are not taken into account. Both emission and absorption processes are included.

IV. TRANSPORT PROBLEM

It is evident from Fig. 4 that very high scattering rates must be expected for the electron energies observed experimentally. Under these conditions, the semiclassical approach to the transport problem (the Boltzmann equation or the equivalent Monte Carlo technique) may suffer from serious difficulties. We now briefly review these problems and describe later, in Sec. IV B, how one of these nonlinear effects, the "collision broadening," has been implemented in our Monte Carlo simulation.

A. Limits of the semiclassical approach

The semiclassical description of electron transport relies on two basic assumptions: the validity of the perturbation theory and of the adiabatic approximation.[36] For perturbation theory to apply, the unperturbed electron must be described by an eigenstate sufficiently stable to survive at least one de Broglie wavelength $\lambda_{\text{de Broglie}}$ before scattering when the perturbing Hamiltonian is turned on; that is

$$l \gtrsim \lambda_{\text{de Broglie}} = 1/k \ , \tag{12}$$

where k is the magnitude of the electron wave vector and l its mean free path.

The adiabatic approximation requires that the electronic wave functions respond instantaneously to the motion of the ions in the crystal. If the phonon wavelength is larger than the electron mean free path, the charge redistribution following a lattice distortion cannot occur and the adiabatic approximation fails. In other words, two successive collisions must be separated by a time interval sufficiently long so that the two processes may be regarded as independent. Otherwise, the interference between the emitted or absorbed phonons may change the strength of the interaction. This condition can be expressed as

$$l \gtrsim 1/q \ , \tag{13}$$

where q is the magnitude of the phonon wave vector. In general, if these conditions are not satisfied, a correct solution of the transport problem can only be obtained by solving the lattice degrees of freedom exactly (i.e., nonperturbatively), as done by Thornber and Feynman for the alkali halides.[6] Unfortunately, their path-integral approach is quite unmanageable in our situation, since more than one lattice mode has to be solved. Thus, in our approach no attempts have been made to solve these difficulties which can arise at high electron energies. A more complete discussion of these issues, given by Peierls[37] and Landau,[38] suggests that actually the limits set by Eqs. (12) and (13) may be too strict and that we could push perturbation

theory, to some extent, beyond those limits. More recently, Capasso *et al.*[39] have pointed out that one should at least account for the fact that when the condition given by Eq. (12) is not met, the eigenstate describing an electron of momentum $\hbar k$ should be given a broadening $\Delta w \approx \hbar/\tau$, τ being the average time between collisions. This accounts for the short lifetime of the states employed in the perturbative expansion and has been implemented in our simulation, as discussed below. However, it should not be viewed as the final solution of these problems.

Another assumption usually made in solving transport problems is to ignore the finite duration of the collision processes. However, at high electric fields the electron energy may change significantly *during the collision process* as it moves in the high external field. As a result, the scattering rates would be significantly altered. Barker[40] has considered the effects of the intracollisional field on the scattering rate and has given a criterion for the validity of the standard perturbation theory in the form

$$\Delta w > \frac{|e\hbar\mathbf{F}\cdot\mathbf{q}\tau_c|}{2m^*} , \tag{14}$$

where $\mathbf{F}$ is the electric field, τ_c is the duration of the collision ($\approx$ the inverse of the phonon frequency), and Δw is the electron-energy broadening mentioned above. Again, this criterion is violated at high energies and for the umklapp processes considered here. Attempts to solve this problem have been made in the past, but it would be a formidable task to implement them in the present context. Finally, the nonpolar electron-phonon scattering rate must eventually drop at electron velocities too high for even the acoustic mode to respond and absorb energy from the traveling carrier.[41] We lack any estimate about the critical energy at which this could happen and will proceed using Eq. (11) at all energies above w_{BZ}.

In conclusion, the experimental data as well as the results of our semiclassical Monte Carlo approach show that, at the fields of interest, most of the electrons in SiO_2 have relatively low energies, so that the scattering rates are sufficiently moderate to give us some confidence about the validity of the semiclassical picture, particularly if proper account is taken for the collision-broadening effects. However, care must be taken when considering the high-energy tails of the electron-energy distributions, since these nonlinear effects become important in this range of energies.

B. Collision broadening

When the average time τ between two successive collisions with the lattice becomes too short, one must assign the electrons a finite linewidth, Δw. From the Heisenberg uncertainty principle, this width is of the order of $\hbar/\tau$ and it changes the scattering rate itself, since the electrons can now scatter to a broadened distribution of final states.

The necessity of including this effect into semiclassical Monte Carlo simulations has been discussed by Capasso *et al.*[39] Chang *et al.*[42] have calculated the effect of the collisional broadening on the electron-phonon scattering rate by relating it to the imaginary part of the electron self-energy via the optical theorem. An easy way to see how this arises[43] is to consider an electron in the unperturbed state (i.e., eigenstate of the free Hamiltonian) $|\mathbf{k}\rangle$ at time t and ask what is the probability that the electron will still be in the same state after a time interval Δt when the electron-phonon interaction (i.e., the perturbing Hamiltonian) is turned on. In the interaction representation of time-dependent perturbation theory, the amplitude for the electron to remain in the same state is

$$\langle \mathbf{k},t+\Delta t \,|\, \mathbf{k},t\rangle = \exp\left[\frac{i}{\hbar}\Delta w_{\mathbf{k}}\,\Delta t\right] , \tag{15}$$

where $\Delta w_{\mathbf{k}}$ is the (complex) energy shift of the state $|\mathbf{k}\rangle$, due to interaction Hamiltonian H_{int}, that is, the electron self-energy. At the lowest order in the perturbative expansion, $\Delta w_{\mathbf{k}}$ is given by

$$\Delta w_{\mathbf{k}} = \sum_{\mathbf{q},\mathbf{k}'} \sum_{\pm} \frac{|\langle \mathbf{k},x_f \,|\, H_{\text{int}} \,|\, \mathbf{k}',x_i\rangle|^2}{w_{\mathbf{k}} - w_{\mathbf{k}'} \pm \hbar\omega_{\mathbf{q}} + \Delta w_{\mathbf{k}}} , \tag{16}$$

where H_{int} is the interaction Hamiltonian at the initial time t. The sum is performed over the intermediate electron and phonon states of momentum $\mathbf{k}',\mathbf{q}$ and energy $w_{\mathbf{k}'},\hbar\omega_{\mathbf{q}}$, respectively, as illustrated in Fig. 6, and over emission ($-$) and absorption ($+$) of one phonon. The labels $x_{i,f}$ represent the proper phonon states in the matrix elements relative to the emission and absorption processes.

The real part of the self-energy represents the energy shift of the state $|\mathbf{k}\rangle$ due to the electron-phonon interaction, while the imaginary part of $\Delta w_{\mathbf{k}}$ expresses the finite electron linewidth. This is related to the lifetime of the state $|\mathbf{k}\rangle$ since, from Eq. (15), the probability that the electron will remain unscattered in the same state after a time Δt is

$$|\langle \mathbf{k},t+\Delta t \,|\, \mathbf{k},t\rangle|^2 = \exp\left[-\frac{2}{\hbar}\text{Im}(\Delta w_{\mathbf{k}})\Delta t\right] . \tag{17}$$

The quantity $2\text{Im}(\Delta w_{\mathbf{k}})/\hbar$ is the lifetime of the electron state, that is, the scattering rate:

$$\frac{1}{\tau(\mathbf{k})} = \frac{2\,\text{Im}(\Delta w_{\mathbf{k}})}{\hbar} . \tag{18}$$

From Eqs. (16) and (18), we finally obtain an equation for the scattering rate:

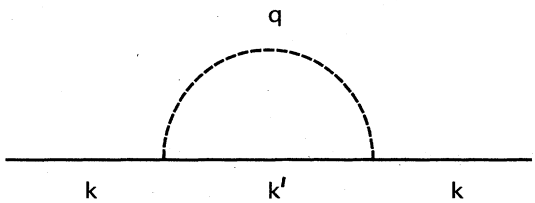

FIG. 6. Diagram illustrating the one phonon emission and/or absorption processes contributing to the self-energy of the electrons.

$$\frac{1}{\tau(\mathbf{k})}=\frac{2}{\hbar}\sum_{\mathbf{q},\mathbf{k}'}\sum_{\pm}|\langle\mathbf{k}',x_f|H_{\rm int}|\mathbf{k},x_i\rangle|^2\frac{\Gamma(\mathbf{k})}{[w_{\mathbf{k}}-w_{\mathbf{k}'}+{\rm Re}(\Delta w_{\mathbf{k}})\pm\hbar\omega_{\mathbf{q}}]^2+[\Gamma(\mathbf{k})]^2}\ , \tag{19}$$

where $\Gamma(\mathbf{k})={\rm Im}(\Delta w_{\mathbf{k}})=\hbar/2\tau(\mathbf{k})$. Equation (19) can now be solved to obtain the scattering rate $1/\tau$. It can be noticed that Eq. (19) can be obtained by the Fermi golden rule simply replacing the energy-conserving δ function with a Lorentzian of half-width Γ.

In high-energy region ($w\gtrsim w_{\rm BZ}$), where collisional-broadening effects are expected to be significant, we can consider only the broadening due to the nonpolar interaction with the band-edge phonons. By using Eq. (19), the scattering rate given by Eq. (11) is replaced by the solution of the equation

$$\frac{1}{\tau_{\rm nonpolar}(w)}\simeq\frac{8\pi^3\hbar^2N^2\sigma}{m^*M_>\omega_{\rm edge}}\left[\frac{w}{w_{\rm BZ}}\right]^{3/2}(2n_{q_{\rm BZ}}+1)\times\left[\frac{2}{\pi}\arctan\left[\frac{8w}{\Gamma}\right]-\frac{\Gamma}{4w}I(w)\right]\ , \tag{20}$$

where account is made for the broadening of both initial and final states by defining $\Gamma=\hbar/\tau_{\rm nonpolar}(w)$, and

$$I(w)=\int_{-1}^{1}dt\frac{t^4(2t+1)}{t^2(t+1)^2+(\Gamma/4w)^2}\ .$$

Equation (20) has been obtained by assuming that $w\gg\hbar\omega_{\mathbf{q}}$ and $\Gamma\gg\hbar\omega_{\mathbf{q}}$, by neglecting the real part of the energy shift $\Delta w_{\mathbf{k}}$, and limiting the sum in Eq. (19) to $q\le k$.

The integral $I(w)$ has been evaluated analytically using the symbolic language Scratchpad[44] and Eq. (20) has been solved numerically to obtain the scattering rate $1/\tau(w)$. Figure 7 shows the result. The low energy ($w<w_{\rm BZ}/2$) and the broadened high-energy scattering rates have been interpolated with a cubic function in this example. The effect of the collision broadening is that of slightly increasing the scattering rate at high energies, as can be seen comparing Fig. 5 to Fig. 7.

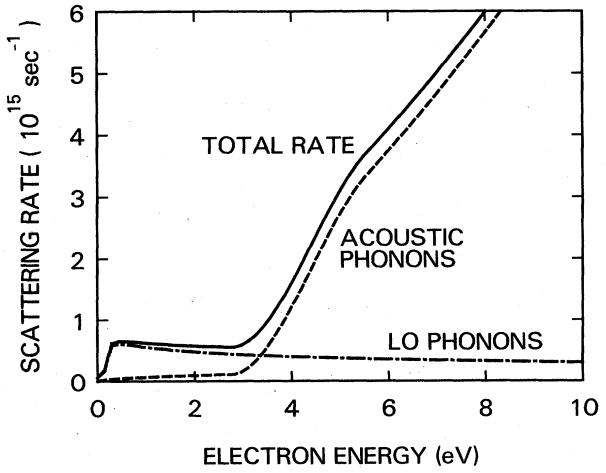

FIG. 7. Electron-phonon scattering rates in SiO_2 at 298 K with the inclusion of collision-broadening effects.

V. MONTE CARLO TECHNIQUE

We have employed a conventional Monte Carlo technique to solve the electron-transport problem in SiO_2. Excellent reviews of this technique have been given by Price[45] and Jacoboni and Reggiani.[46] Here, we briefly summarize the basic issues and their implementation in our work.

A. Technique

1. Duration of the electron free flight

When simulating the electron transport in a uniform electric field, the position and momentum of the electrons during the free flights between collisions have been determined by solving directly the classical equations of motion. If nonuniform fields were considered, as in the simulation of internal photoemission, a second-order Runge-Kutta algorithm was used.

In order to determine stochastically the time t during which the electron will move free in the solid, we must consider the probability $p(t)dt$ that an electron will suffer a collision during a time interval dt after having traveled freely for a time t and having undergone the previous collision at time $t=0$. Knowing the total scattering rate $1/\tau(\mathbf{k})$ as a function of the electron wave vector (or of its energy, as in the case of spherical bands), this can be written as

$$p(t)dt=\frac{dt}{\tau(\mathbf{k}(t))}\exp\left[-\int_0^t dt'\frac{1}{\tau(\mathbf{k}(t'))}\right]. \tag{21}$$

The evaluation of the integral in the exponent can be very time consuming. Therefore, we have employed a standard technique, called a "self-scattering" algorithm.[47] It consists in defining a "fake" total scattering rate $1/\tau_0$ which constitutes an upper bound to the real total scattering rate in the region of energy of interest. Then, Eq. (21) becomes trivially

$$p(t)dt=\frac{1}{\tau_0}\exp(-t/\tau_0)\ , \tag{22}$$

and the time of free flight t until the next collision can be obtained from a random number ξ_1 in the interval [0,1] as $t=-\tau_0\ln(\xi_1)$. One must take into consideration that some computer time must be wasted to decide whether the electron has undergone a real or a fake collision. A second random number ξ_2 is generated. If $\xi_2>\tau_0/\tau(w)$, then a self-scattering event has taken place and the final electron state is taken equal to the initial state. Otherwise, the collision process is considered.

2. Determination of the collision process

The same random number ξ_2 is employed to determine the type of interaction the electron suffers by comparing it with the partial scattering rates:

$$a_1 = 1/\tau_1(w) ,$$
$$a_2 = 1/\tau_1(w) + 1/\tau_2(w) ,$$
$$\ldots ,$$
$$a_n = a_{n-1} + 1/\tau_n(w) ,$$

where $1/\tau_1$, $1/\tau_2$, etc., are the various types of collisions. If $a_i < \xi_2/\tau_0 < a_{i+1}$, then the ith collision process has taken place. To further reduce the computing time, the quantity $1/\tau_0$ can be considered to be a function of the electron energy, so that the probability of having a fake collision is always very small. This "fast self-scattering" algorithm can be implemented by calculating the scattering rates at several electron energies separately from the main program and storing them in a separate file. For a given electron energy, the scattering rate is read from this file with a suitable interpolation and the constant τ_0 is estimated so that it is always larger than the total scattering rate. A check must be made that during the free flight the electron energy does not increase so much that the total scattering rate exceeds $1/\tau_0$. If this occurs, the constant τ_0 is decreased and the free flight repeated. The reduction in computer time this procedure provides is particularly large when the collision-broadening effects are included, since the calculation of the scattering rates themselves requires a significant computing time.

3. Determination of the final state after scattering

The final state of the scattered electron is determined by the polar and azimuthal scattering angles, θ and ϕ, and by its new energy. The algorithm employed to choose them stochastically is originally due to Metropolis and Ulam.[48] If x is a random variable having probability $p(x)dx$ of taking a value between x and $x+dx$, then a random choice of x preserving its probability distribution is obtained by choosing a random number ξ with uniform distribution in the closed interval [0,1], and solving the equation

$$P(x) = \frac{\int_{x_{\min}}^{x} dx' p(x')}{\int_{x_{\min}}^{x_{\max}} dx' p(x')} = \xi . \tag{23}$$

If the probability $P(x)$ is not an easily invertible function, the rejection technique[49] can be employed to save computing time. A number M is selected, such that $M \geq p(x)$ in the interval $[x_{\min}, x_{\max}]$. Then, after selecting two random numbers ξ and η in [0,1]. $X = p[x_{\min} + \xi(x_{\max} - x_{\min})]$ and $Y = \eta M$ are compared. If $X \geq Y$, then the value $x' = x_{\min} + \xi(x_{\max} - x_{\min})$ is chosen. Otherwise, a new pair of numbers ξ and η are selected and the procedure repeated. Obviously, the values x' chosen in this way will be distributed between $x_{\min}$ and $x_{\max}$ with probability p.

Therefore, after having selected the type of collision, the magnitude of the wave vector q of the absorbed or emitted phonon is chosen with either technique. Typically, since the probability distributions of the phonon wave vectors, as given by the integrands of Eqs. (4) and (9), are easily integrated and inverted, the direct technique is employed. After having determined q, the polar scattering angle θ is easily calculated from energy and momentum conservation.

The polar scattering angle θ is simply chosen randomly from a random number ξ_3 in [0,1]:

$$\cos\theta = 1 - 2\xi_3 , \tag{24}$$

in the occurrence of umklapp processes, as some momentum is also transferred to the lattice in the Bragg reflection accompanying these processes. The azimuthal angle ϕ is also chosen randomly between 0 and 2π.

Finally, the energy of the emitted or absorbed phonon is known either because the dispersion is ignored (LO and band-edge phonons) or from the value of q previously determined. Thus, the energy of the scattered electron can be selected. Its new velocity and direction are finally obtained from the energy-momentum dispersion relation (parabolic in our approximation) and from simple trigonometric relations.

4. Collision broadening

If collision broadening is introduced, then the final energy of the electrons is chosen via the rejection technique with a Lorentzian probability centered around the classical value and with half-width Γ, as discussed previously. The same procedure should be followed to select the phonon wave vector q, and thus θ. In practice, since the broadening effects are significant in the high-energy region (i.e., the region in which most of the collisions involve umklapp processes), the broadening of the final angles is ignored, and θ is selected randomly, as in Eq. (24).

B. Determination of the physical quantities

The Monte Carlo technique allows the determination of quantities of physical interest such as electron-energy distributions, average energies, and drift velocities. In a steady-state situation, these can be determined by following a single electron traveling in the solid, sampling periodically its position, time of flight and momentum, and averaging them.

In our case, the existence of a steady-state transport was not *a priori* obvious, particularly in the light of the results of Fitting and Frieman. Therefore, the histories of a statistically high number of independent electrons were simulated over a prefixed distance (the oxide thickness). Even when the existence of a steady-state regime is asserted, this allows also the simulation of transient situations, as those occurring over distances too short to attain steady state, or in internal photoemission, when nonuniform external fields are present. The possibility of solving with minor efforts the transport equation even in a transient regime is actually one of the main advantages of the Monte Carlo technique.

The energy-distribution histograms and average energies were obtained by simply recording the energies at the end of the travel. The ergodic theorem guarantees that this is the correct procedure at steady state. Drift velocities were obtained by selecting a fixed travel distance, suf-

ficiently far from the starting position so to guarantee the achievement of a steady-state regime. For every free path around this position, its length and duration were recorded and the drift velocity obtained directly from the ratio of the average path length over the average path duration. An alternative estimator[45] of the drift velocities was also obtained by recording the change of electron energy during each path, Δw, and the change of the component of the electron momentum along the field $\mathbf{F}$, $\hbar\Delta k_F$. The average drift velocity $\langle v_D \rangle$ was then obtained from a sum of these quantities over all paths around the chosen position:

$$\langle v_D \rangle = \frac{\sum_{\text{paths}} \Delta w}{\sum_{\text{paths}} \hbar \Delta k_F} . \tag{25}$$

The Monte Carlo program has been written in FORTRAN77 and run on an IBM, model No. 3081 computer. Electron-energy distributions and average energies were obtained by following the histories of 500 to 2000 electrons over a typical distance of 50 nm. Larger distances were occasionally tried to check the stability of the distributions. Shorter distances were employed to determine the minimum length that the electrons must travel to reach a steady-state condition. The initial electron states were selected by choosing zero forward angle and zero energy, as in a Fowler-Nordheim tunnel-injection experiment. Occasionally, nonzero initial energies and randomly selected forward angles were employed to determine the "cooling" or "heating" distance as a function of the initial electron energy and field. Typically, the computer time required to obtain a 500-electrons histogram was about 10 min of CPU (central processing unit) time at low fields ($\simeq 4\times 10^6$ V/cm), increasing to 20 min or more at the high fields at which more frequent scattering at larger angles occurs ($\gtrsim 8\times 10^6$ V/cm).

VI. RESULTS OF THE SIMULATION

A. Steady-state transport in uniform field

Figure 8 shows the energy distributions obtained with and without the inclusion of the collisional broadening for electrons traveling in a uniform field. The travel length was 50 nm for both the Monte Carlo simulation and the experimental data shown for comparison.

The average electron energy which is deduced from these distributions is plotted in Fig. 9 as a function of the electric field. We have also reproduced the experimental data obtained from the three experimental techniques described in Sec. II D. Figure 10 illustrates the fact that, depending on the applied field, a relatively short distance is needed to attain a steady-state situation. Electrons starting with zero energy will, on the average, gain significant energy in the first few nm. At high ($\gtrsim 6\times 10^6$ V/cm) and low fields ($\lesssim 2\times 10^6$ V/cm), the average electron energy corresponds to high scattering rates, as can be seen from Fig. 5 or Fig. 7. Therefore, a short "heat-up" distance (≈ 1 to 4 nm) is sufficient to achieve a steady-state distribution. In the range of medium fields, the

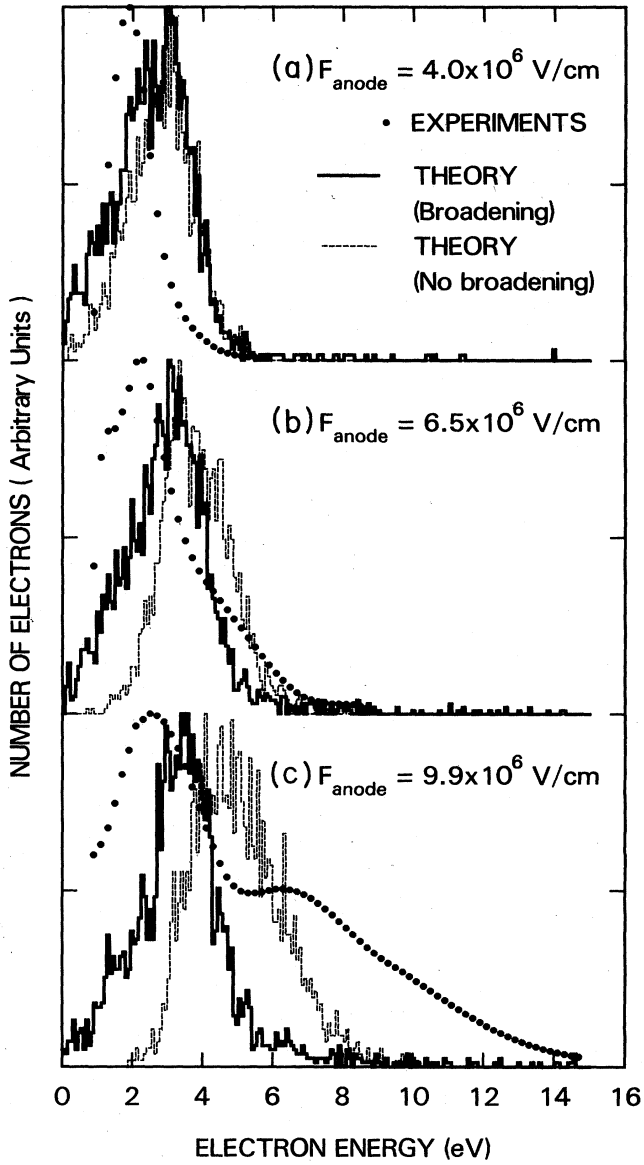

FIG. 8. Electron-energy distributions at three different values of the anode field as obtained from vacuum-emission experiments described in Ref. 3 and from the Monte Carlo simulations with and without collision-broadening effects.

average energy corresponds to a minimum of the scattering rates, the LO phonons having already lost their efficiency, but the acoustic phonons still providing a relatively weak interaction. Thus, longer field-thermalization distances, approaching 10 nm, are obtained. After the electrons have traveled 1 to 10 nm, the average energy relative to the uniform field in the oxide is obtained and transport occurs in a steady-state regime. Simulations performed for travel distances as long as 150 nm have shown that the average energies do not vary, while only a slight increase in the high-energy tail of the distribution is observed as the distance increases. The "cool-down" distance (that is, the distance electrons injected with high energy have to

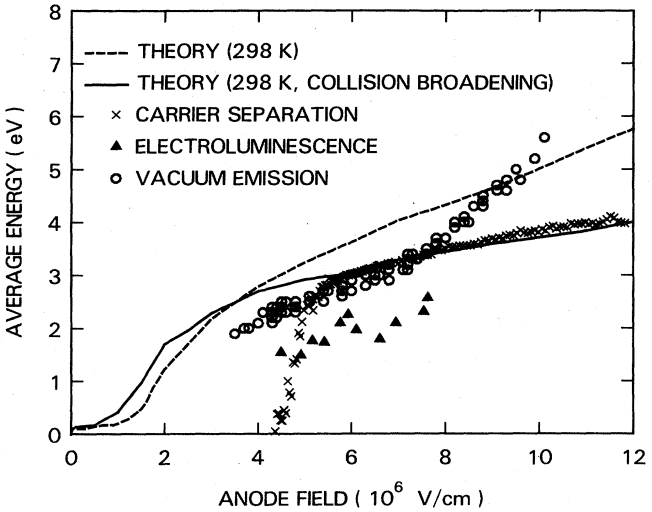

FIG. 9. Average electron-energy obtained from the Monte Carlo simulations (with and without collision-broadening effects) as a function of the anode fields. Comparison is made with the data of Fig. 4 replotted by measuring the energy from the bottom of the SiO_2 conduction band. The Monte Carlo data are obtained by simulating the transport of 2000 electrons across 50 nm of SiO_2. The statistical error is less than ± 0.05 eV at the higher fields. An effective mass $m^*=m_{\text{free}}$ has been employed at all energies. Simulations performed employing an energy-dependent effective mass ($m^*=0.5m_{\text{free}}$ at low energy, $m^*=m_{\text{free}}$ at high energies, as described in Ref. 8) have provided similar results for fields larger than 2×10^6 V/cm, the average energy being slightly higher at the lower fields.

travel to reach the steady-state regime) is illustrated in Fig. 11. Again, this distance is a function of both the initial electron energy and the electric field.

These field-thermalization characteristic distances are

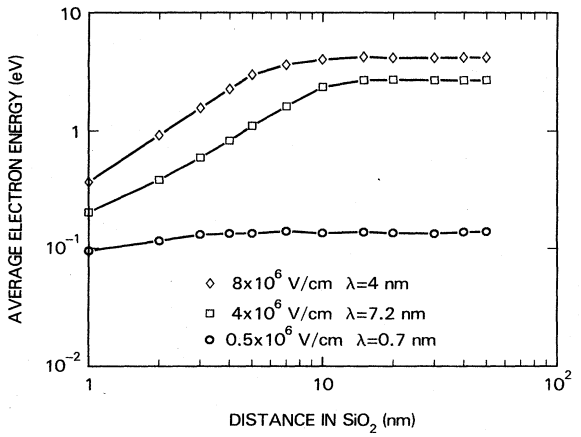

FIG. 10. Simulated average energy of electrons injected with zero initial energy into SiO_2 as a function of distance inside the oxide at three values of the electric field (no collision broadening). The energy-relaxation distance λ has been obtained by fitting the data to the expression $\langle w(x)\rangle=\langle w(\infty)\rangle[1-\exp(-x/\lambda)]$, where x is the distance inside the SiO_2 and $\langle w(\infty)\rangle$ the average energy of the electrons in the steady-state regime in the applied field.

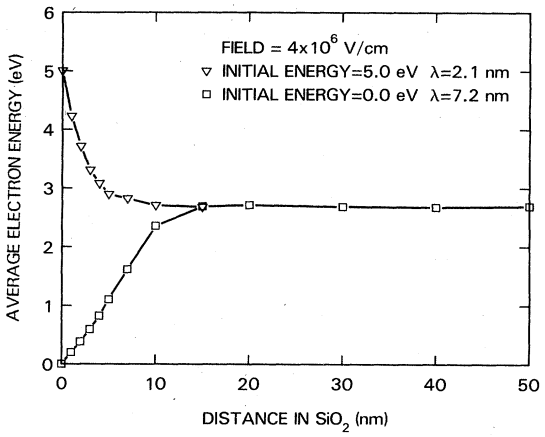

FIG. 11. Simulated average energy of electrons injected with 0 and 5 eV initial energy as a function of the distance inside the SiO_2 (no collision broadening). The energy-relaxation distance λ has been obtained by fitting the data to the expression $\langle w(x)\rangle=\langle w(\infty)\rangle+(w_i-\langle w(\infty)\rangle)\exp(-x/\lambda)$, where w_i is the initial electron energy.

strictly related to the so-called "energy-relaxation length" usually employed to linearize the Boltzmann equation.[24] The "energy-relaxation time" τ_w is usually defined as

$$\tau_w=\frac{|\langle w\rangle-\langle w_0\rangle|}{\langle v_D\rangle eF}\ , \tag{26}$$

where $\langle w_0\rangle$ is the average initial electron energy (the thermal equilibrium or the injection energy) and $\langle w\rangle$ is the average energy at steady state in presence of the field. The energy-relaxation distance is then

$$\lambda=\langle v_D\rangle\tau_w=\frac{|\langle w\rangle-\langle w_0\rangle|}{eF}\ . \tag{27}$$

The results providing rather short relaxation distances imply that in the case of electric fields distorted by oxide charging (such as, electron trapping), the electron-energy distributions will be completely determined by the value of the electric fields close to the positive electrode; that is, the *anode* field. Therefore, comparison between theoretical and experimental results should be done at the same value of the anode field. This has been done in Figs. 8 and 9.

The energy-relaxation distance can also be related to the characteristic slope of the curve $\langle w\rangle$ versus F in the range of electric field for which the average energy increases linearly with the field,[50] as indicated by Eq. (1). The constant λ is found to be approximately 3.5 nm when no account is made for the collisional-broadening effects, and 2 nm if the broadening is included in the simulation. These values agree well with the experimental values obtained by the different techniques previously discussed.

The satisfactory agreement between the experimental data and the results of the Monte Carlo simulation, which has been reported previously, is significantly improved by the inclusion of the collisional broadening. We should be cautious in concluding that this broadening solves the problems of the semiclassical picture. After all, the non-

polar scattering rate is calculated by estimating rather crudely the coupling constant S_q/q. Even in well-known semiconductors, such as Si and GaAs, these coupling constants are treated as adjustable parameters and determined by fitting the theory to the experimental data.[51] A similar procedure could have been employed in this work. Therefore, the only conclusion we can draw is that the collision broadening seems to provide a better agreement between experiment and theory with our particular choice for the coupling constant of the nonpolar electron-phonon interaction. But other choices of this constant may provide opposite results. An independent determination of the form factor of SiO_2, either experimental or theoretical, is needed before stronger conclusions could be drawn.

The main conclusion of the simulation can be cast in the following form. The LO phonons are able to maintain a stable electron-energy distribution as long as the field is lower than the critical value $F_{th} \simeq 1.5 \times 10^6$ V/cm. The strong polar interaction and the large energy losses with the 0.15-eV phonons keep the electrons almost thermal. This confirms the validity of the standard LO-phonon—based picture at these low fields. However, above F_{th} the LO phonons are unable to prevent the velocity runaway. This can be seen from the sharp increase of the average energy at about 1×10^6 to 1.5×10^6 V/cm in Fig. 9. Indeed, without the inclusion of the nonpolar scattering, a steady-state situation cannot be obtained. At fields higher than F_{th}, the nonpolar scattering dominates the transport. Its main effect is that of randomizing the electron momenta via the large-angle scattering, particularly in the umklapp processes.[52] This is evident from Fig. 12, where a comparison is made between the low-field trajectories (dominated by forward scattering with LO phonons) and the high-field trajectories (affected by the many Bragg reflections and large-angle scattering involved in nonpolar collisions). Thus, the actual electron paths get longer as the field increases. Although the energy absorbed by the acoustic phonons is practically negligible, the longer paths produce an enhanced probability of energy losses to the LO phonons and the electron distributions remain stable at all the fields at which the simulation was performed ($\lesssim 1.6 \times 10^7$ V/cm). The problems which affect our semiclassical approach at high electron energies should not change the basic features of this picture. Indeed, the mean free path of an average electron ranges from about 1.5 nm at 3 eV (4×10^6 V/cm) to about 0.8 nm at 4 eV (12×10^6 V/cm); that is, it is sufficiently long to satisfy the requirements set by Eqs. (12) and (13). However, a comparison between the theoretical and experimental electron-energy distribution shown in Fig. 8 indicates that at high energies the scattering rate may be lower than predicted by Eqs. (11) or (20). In particular, the strong high-energy tails observed in vacuum-emission experiments may originate from the low density of states at the edge of the first Brillouin zone, as confirmed by inverse-photoemission data,[53] and from the nonparabolicity of the SiO_2 conduction band at these high energies.[32] Stronger conclusions cannot be drawn, as we should regard the vacuum-emission data as also affected by some uncertainty, since it is not easy to estimate to what extent the experimental distributions are distorted by the thin

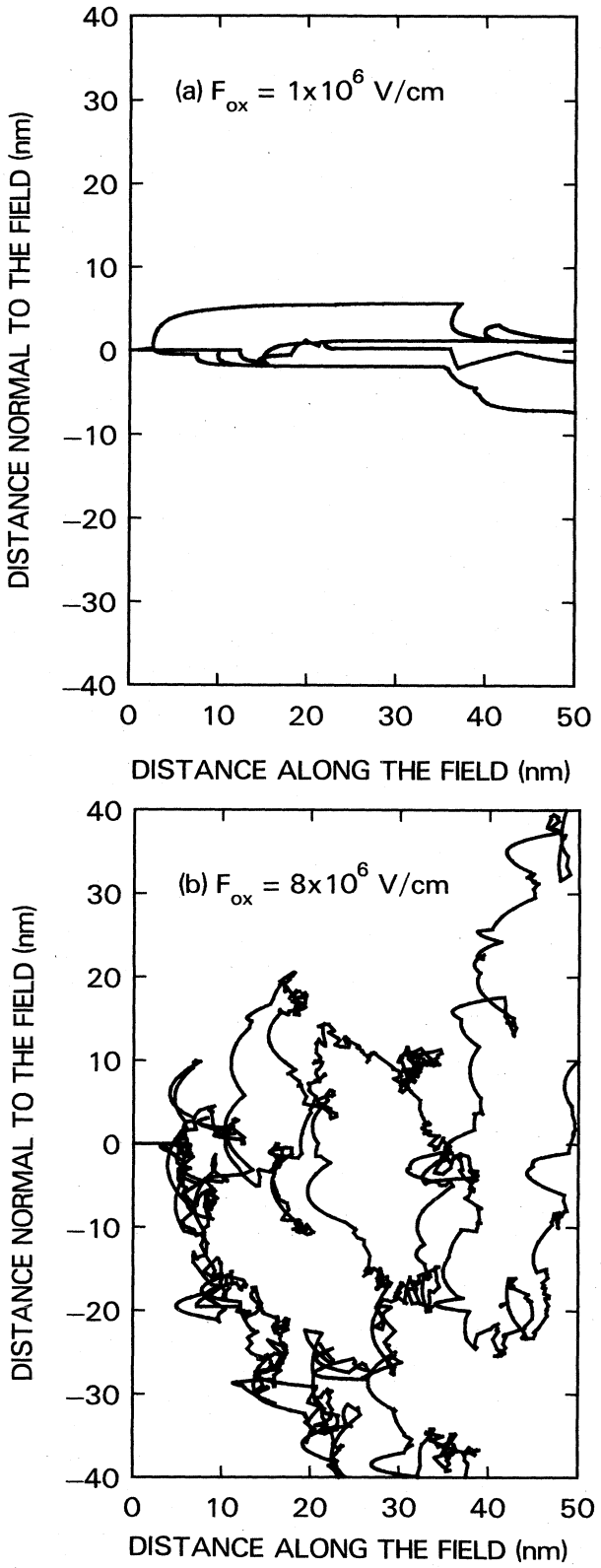

FIG. 12. Trajectories of four electrons in real space at two values of the electric field. The low-field trajectories show that the transport is dominated by the forward polar scattering, while at 8×10^6 V/cm the nonpolar scattering at large angles randomizes the direction of motion.

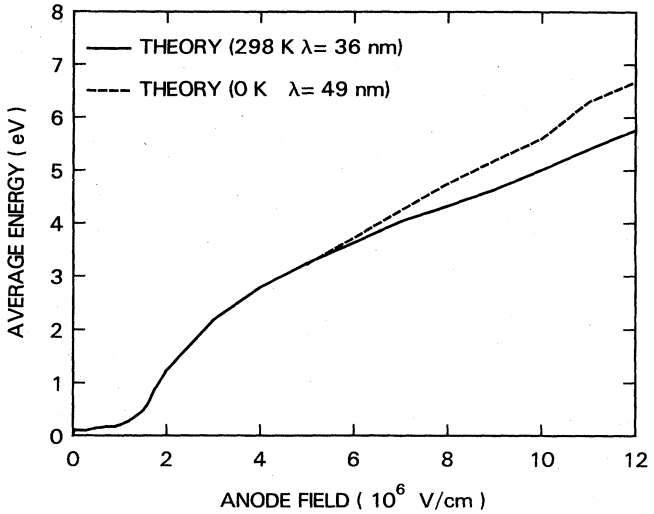

FIG. 13. Simulated average energy of electrons at 0 and 298 K without collision-broadening effects. At room temperature and high fields the electrons attain a lower energy since they suffer a larger number of collisions with the more numerous acoustic and band-edge phonons.

metal gate.[3]

The effect of the lattice temperature on the average electron energies has been simulated by considering only the emission processes by setting $n_{LO}=0$ in Eq. (5) and $n_q=0$ in Eqs. (9) and (11), thus simulating transport at 0 K. The average electron energies at 0 and 298 K are shown in Fig. 13. As expected, no appreciable differences are observed at the low fields at which the electron transport is controlled by the high-energy LO phonons whose population is weakly dependent on temperature. At high fields and low temperature, the nonpolar scattering with the less numerous acoustic and band-edge phonons is significantly reduced and the average energies increase, although the effect is not large.

Finally, we show in Fig. 14 the average drift velocity as a function of the field. In the LO-phonon—controlled regime, our results reproduce those obtained by Ferry. Agreement between theory and the experimental results of Hughes can be obtained by assuming a much larger electron effective mass ($\gtrsim 1.3 m_{free}$) which would result from the formation of a polaron at low fields.[54] At higher fields, the polaron should be "stripped" and the bare electron mass should be recovered. A saturation of the drift velocity is observed as soon as the nonpolar scattering takes over. Actually, a negative differential mobility seems to occur at high fields, probably due to the longer time spent by the carriers in the insulator as the probability of large-angle scattering and umklapp processes becomes significant.

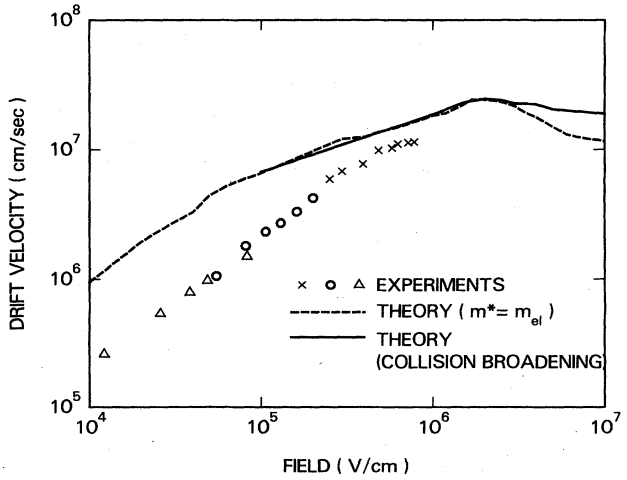

FIG. 14. Simulated room-temperature drift velocity as a function of the electric field with and without the inclusion of collision broadening. The experimental data are taken from Ref. 14.

B. Internal photoemission

In the experiments aimed to determine the yield of internal photoemission, ultraviolet light ($\simeq$5 eV) is used to excite carriers from below the Fermi level of the electrodes of an MOS capacitor. Since the barrier at the SiO_2-electrode interface for the holes is usually much larger than the barrier for electrons, only electrons can be injected from either electrode by choosing the proper polarity of the bias voltage applied to the gate of the structure. The photocurrent flowing through the insulator is then measured as a function of the photon energy for a fixed value of the bias voltage or, for fixed photon energy, as a function of the field applied to the insulator.

In order to interpret the data collected in the past, account must be made for the lowering of the SiO_2-electrode potential barrier due to the image force. The potential

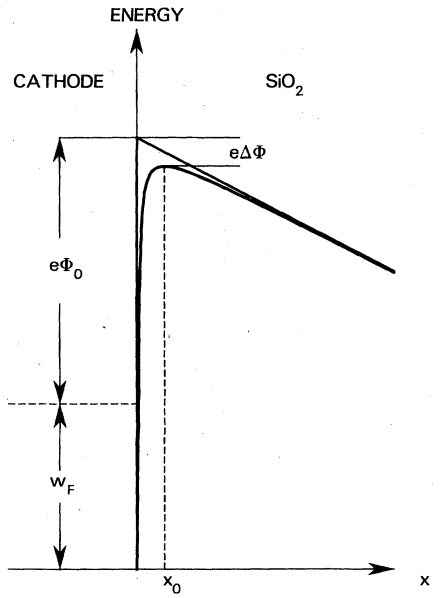

FIG. 15. Schematic representation of the potential at the cathode-SiO_2 interface (with image-force barrier lowering) which has been used in the simulation of internal photoemission experiments.

$\Phi(x)$ at a distance x inside the SiO_2 from the injecting interface can be written as

$$\Phi(x)=\Phi_0-Fx-\frac{e}{16\pi\epsilon_{ox}x}\ , \tag{28}$$

where Φ_0 is the barrier height in absence of image force, ϵ_{ox} is the SiO_2 permittivity, and F is the uniform field applied externally across the insulator. As illustrated in Fig. 15, the potential has a maximum at

$$x_0=\left[\frac{e}{16\pi\epsilon_{ox}F}\right]^{1/2}, \tag{29}$$

and the barrier height is reduced by the amount

$$\Delta\Phi=\left[\frac{eF}{4\pi\epsilon_{ox}}\right]^{1/2}. \tag{30}$$

In their early experiments, Berglund and Powell[16] could explain their data by assuming that the electrons excited above the barrier maximum could scatter in the barrier with an effective escape distance λ and be reflected into the injecting electrode. The photoyield Y could be well fitted by the following equation:

$$Y=A\exp(-x_0/\lambda)(\hbar\omega-\Phi_0+\Delta\Phi)^p\ , \tag{31}$$

where p is an integer taking a value between 2 and 3, depending on the energy distribution of the electrons excited in the cathode, $\hbar\omega$ is the photon energy, and A is a function of the photon frequency which reflects the properties of the photon absorption in the cathode. The characteristic distance λ deduced from the experiments had a value of about 2.5–3.5 nm. This value could not be accounted for by the standard picture.

We have performed several Monte Carlo simulations of this process. The photoexcitation of the electrons by photons of energy $\hbar\omega$ has been simulated by employing the potential given by Eq. (28) and avoiding the singularity at $x=0$ by truncating the potential at the Fermi level of the cathode. The initial electron energy w_i was randomly selected between the Fermi level of the cathode, w_F, and $w_F+\hbar\omega$, that is

$$w_i=w_F+\xi\hbar\omega\ , \tag{32}$$

ξ being a random number between 0 and 1. The azimuthal injection angle is selected randomly. The polar angle θ in the electrode is also selected randomly:

$$\cos\theta=1-2\xi_\theta\ . \tag{33}$$

However, this angle will be modified by the refraction that the electrons suffer as they enter the insulator, becoming

$$\theta_{ox}=\arccos\left[\left[\frac{(w_F+w_{i,ox})(1-2\xi_\theta)^2-w_F}{w_{i,ox}}\right]^{1/2}\right], \tag{34}$$

where $w_{i,ox}$ is the initial electron energy measured from the Fermi level of the cathode. One restriction applies to the values θ can have, as it follows from Eq. (34):

$$(w_F+w_{i,ox})\cos^2\theta-w_F>0\ , \tag{35}$$

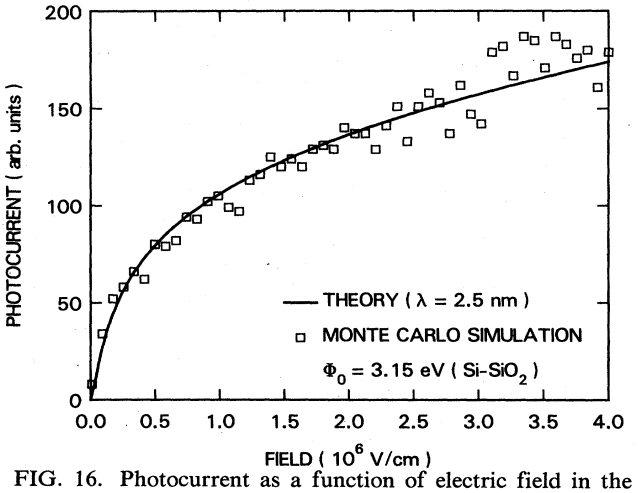

FIG. 16. Photocurrent as a function of electric field in the SiO_2 as obtained from the Monte Carlo simulation without collision-broadening effects. The photon energy employed in the simulation was 5 eV. The numerical results are fitted to the approximate expression given by Ref. 16 and Eq. (32) of the text.

which requires that only electrons having a sufficiently high component of momentum perpendicular to the cathodic interface, $k_\perp$, will enter the oxide; that is, $k_\perp/2m=w_\perp>w_F$.

We show in Figs. 16 and 17 the results of the simulation. We have taken $w_F=12$ eV, as done by Powell and Berglund in the case of injection from the silicon sub-

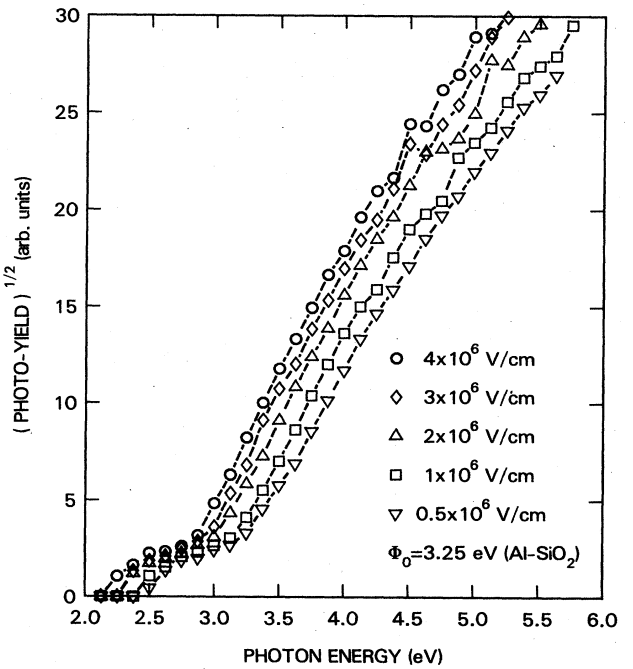

FIG. 17. Square root of the photocurrent is plotted as a function of photon energy for different values of the field in the SiO_2. No collision-broadening effects were included in the simulation.

strate. To obtain the photoyield, electrons reentering the cathode after their injection have been considered reflected and lost. Carriers reaching a distance $2x_0$ inside the insulator have been considered injected. The photoyield as a function of the electric field (Fig. 16) has been fitted with the formula given by Eq. (31) with $p=2$, as follows from the flat electron distribution we have assumed in the cathode. The effective distance λ takes a value of about 2.5 nm, in good agreement with the experimental results. In Fig. 17 we plot the photoyield as a function of the photon energy for the case of injection from the Al electrode ($w_F=10$ eV). The square root of the photoyield is a linear function of $\hbar\omega$, as follows from Eq. (31) with $p=2$. The presence of a tail of the yield at low photon energies should be noticed. These tails have been observed experimentally by Hartstein *et al.*[55] and are too large to be attributed to tunneling phenomena. Their appearance in the simulation is due to the appreciable probability that the electrons absorb energy from the acoustic phonons. Stronger tails could also be expected from the collisional broadening (which has not been included in the results presented in Fig. 17), in analogy to what was found by Tang and Hess.[56]

VII. CONCLUSIONS

In conclusion, by employing a Monte Carlo technique, we have demonstrated that the recent experimental results showing anomalous electron heating in SiO_2 can be explained by invoking the nonpolar electron-phonon interaction. While the LO phonons can indeed control the electron transport at low electric fields, they cannot prevent the velocity runaway at fields as low as 2×10^6 V/cm. Above this critical field, a steady-state electron transport at relatively high average electron energies is provided by the large-angle collisions with the acoustic and band-edge phonons.

Several problems further complicate the results because at high electron energies the semiclassical solution provided by the Monte Carlo technique seems to lose its validity. However, at the average energies observed experimentally and theoretically in the range of 2×10^6 to 12×10^6 V/cm, the scattering rates are sufficiently low to justify use of the semiclassical approach, particularly if proper account is made for the finite linewidth acquired by the electrons. Excellent agreement between the experimental data and the results of the Monte Carlo simulation is obtained, when focusing on the average energies, the energy-relaxation length, and the low-field internal photoemission yields. Thus, the first-order properties of high-field electron transport in SiO_2 seem to be well explained by both polar and nonpolar electron-phonon collisions. On the other side, the results of the vacuum-emission experiments show the existence of a larger number of electrons in the high-energy tail of the distributions than predicted by the semiclassical solutions. This may be an indication that density-of-states, nonparabolicity, and quantum effects begin to take place. More sophisticated approaches—such as those proposed by Thornber and Feynman,[6] Thornber,[57] or Barker[40]—and a better knowledge of the band structure of SiO_2 are needed to obtain a reliable description of these high-energy electrons which may be responsible for the degradation and breakdown of silicon dioxide.

ACKNOWLEDGMENTS

The authors would like to thank P. J. Price for fruitful discussions about the Monte Carlo method and K. K. Thornber for having pointed out some problems relative to the nonpolar electron-phonon scattering at high electron energies. The authors also thank J. Socha for having remarked on the importance of the momentum-randomization effects in controlling the electron transport at high fields, and F. J. Himpsel for a discussion of the inverse photoemission data. Finally, one of us (M.V.F.) deeply appreciates the help provided by Z. A. Weinberg in understanding the problem of hot electrons in SiO_2 (in particular, the inconsistency of the photoemission and resonant tunneling data discussed in Sec. II C with the standard model), and the assistance given by B. M. Trager with the use of the symbolic language Scratchpad II.

*Present address: Massachusetts Institute of Technology, Cambridge, MA 02139.

[1]T. N. Theis, J. R. Kirtley, D. J. DiMaria, and D. W. Dong, Phys. Rev. Lett. **50**, 750 (1983); in *Insulating Films on Semiconductors,* edited by J. F. Verveij and D. R. Wolters (North-Holland, Amsterdam, 1983), pp. 134—140; T. N. Theis, D. J. DiMaria, J. R. Kirtley, and D. W. Dong, Phys. Rev. Lett. **52**, 1445 (1984).

[2]D. J. DiMaria, T. N. Theis, J. R. Kirtley, F. L. Pesavento, D. W. Dong, and S. D. Brorson, J. Appl. Phys. **57**, 1214 (1985).

[3]S. D. Brorson, D. J. DiMaria, M. V. Fischetti, P. M. Solomon, and D. W. Dong, J. Appl. Phys. (to be published).

[4]Massimo V. Fischetti, Phys. Rev. Lett. **53**, 1755 (1984).

[5]H. Fröhlich, Proc. R. Soc. London, Ser. A **160**, 230 (1937); **172**, 94 (1939); Adv. Phys. **3**, 325 (1954). Other early papers are by H. B. Callen, Phys. Rev. **76**, 1394 (1949); and R. Stratton, Proc. R. Soc. London, Ser. A **246**, 406 (1958).

[6]K. K. Thornber and Richard P. Feynman, Phys. Rev. B **1**, 4099 (1972).

[7]L. H. Holway and D. W. Fradin, J. Appl. Phys. **46**, 279 (1975).

[8]M. Sparks, D. L. Mills, R. Warren, T. Holstein, A. A. Maradudin, L. J. Sham, E. Loh, and D. F. King, Phys. Rev. B **24**, 3519 (1981).

[9]W. T. Lynch, J. Appl. Phys. **43**, 3274 (1972).

[10]D. K. Ferry, Appl. Phys. Lett. **27**, 689 (1975); J. Appl. Phys. **50**, 1422 (1979); and in *The Physics of SiO_2 and Its Interfaces,* edited by Sokrates T. Pantelides (Pergamon, New York, 1979), pp. 29—34.

[11]T. H. DiStefano and M. Shatzkes, Appl. Phys. Lett. **25**, 685 (1974).

[12]P. Solomon and N. Klein, Solid State Commun. **17**, 1397 (1975).

[13]R. C. Hughes, Phys. Rev. B **15**, 2012 (1977).

[14]R. C. Hughes, Phys. Rev. Lett. **26**, 1333 (1973); Solid-State Electron. **21**, 251 (1978).

[15]The generation of positive charge in SiO_2 during high-field

electron injection has been investigated so intensively in the past decade that we cannot attempt to cover the literature on the subject. Examples of investigations which lead to a direct correlation between the so-called "anomalous positive charge" and impact ionization can be found in the early paper by Morris Shatzkes and Moshe Av-Ron, J. Appl. Phys. **47**, 3192 (1976) and, more recently, by M. Knoll, D. Braunig, and W. R. Fahrner, IEEE Trans. Nucl. Sci. **NS-29**, 1471 (1982).

[16]C. N. Berglund and R. J. Powell, J. Appl. Phys. **42**, 573 (1971).

[17]J. Maserjian and N. Zamani, J. Appl. Phys. **53**, 559 (1982).

[18]P. Solomon, in *The Physics of SiO_2 and Its Interfaces,* edited by Sokrates T. Pantelides (Pergamon, New York, 1978), pp. 35–39.

[19]T. H. Ning, J. Appl. Phys. **47**, 3230 (1976); D. J. DiMaria, F. J. Feigl, and S. R. Butler, Phys. Rev. B **11**, 5023 (1975); D. J. DiMaria, in *The Physics of SiO_2 and Its Interfaces,* edited by Sokrates T. Pantelides (Pergamon, New York, 1978), pp. 160–178.

[20]A more complete discussion of this issue is given in Ref. 2, where destructive breakdown was observed to occur at anode fields of $(12-16)\times 10^6$ V/cm. Examples of even higher breakdown fields in thin oxides and of the importance of technological variables can be found in Simon S. Cohen, J. Electrochem. Soc. **130**, 929 (1983).

[21]M. V. Fischetti, Z. A. Weinberg, and J. A. Calise, J. Appl. Phys. **57**, 418 (1985).

[22]J. R. Kirtley, T. N. Theis, J. C. Tsang, and D. J. DiMaria, Phys. Rev. B **27**, 4601 (1983).

[23]R. C. Alig, S. Bloom, and C. W. Struck, Phys. Rev. B **22**, 5565 (1980).

[24]K. Seeger, *Semiconductor Physics* (Springer, Vienna, 1983), p. 46.

[25]H.-H. Fitting and J.-U. Frieman, Phys. Status Solidi A **69**, 349 (1982).

[26]J. D. Jackson, *Classical Electrodynamics,* 2nd ed. (Wiley, New York, 1975), p. 618.

[27]B. K. Ridley, J. Appl. Phys. **46**, 998 (1975).

[28]W. A. Harrison, in *The Physics of SiO_2 and Its Interfaces,* edited by Sokrates T. Pantelides (Pergamon, New York, 1978), pp. 105–110.

[29]See, for instance, C. Kittel, *Quantum Theory of Solids* (Wiley, New York, 1963), pp. 130–142; or J. M. Ziman, *Principles of the Theory of Solids* (Cambridge University Press, Cambridge, 1972), p. 205.

[30]J. Bardeen and W. Shockley, Phys. Rev. **80**, 72 (1950).

[31]W. A. Harrison, Phys. Rev. **104**, 1281 (1956).

[32]James R. Chelikowsky and M. Schlüter, Phys. Rev. B **15**, 4020 (1977).

[33]R. W. G. Wyckoff, *Crystal Structure* (Interscience, New York, 1965), and references therein.

[34]S. T. Pantelides and W. A. Harrison, Phys. Rev. B **13**, 2667 (1976).

[35]*Handbook of Chemistry and Physics* (Chemical Rubber Company, Boca Raton, Florida, 1981), 61st edition.

[36]Here, we shall outline the discussion presented by J. M. Ziman, *Electrons and Phonons* (Clarendon, Oxford, 1960), p. 212.

[37]R. E. Peierls, *Quantum Theory of Solids* (Oxford University Press, Oxford, 1974), p. 140.

[38]The argument due to Landau is discussed in R. E. Peierls, Helv. Phys. Acta **7** (Suppl.), 24 (1934).

[39]F. Capasso, T. P. Pearsall, and K. K. Thornber, IEEE Electron Device Lett. **EDL-21**, 295 (1981).

[40]J. R. Barker, J. Phys. C **6**, 2663 (1973), and Solid-State Electron. **21**, 267 (1978).

[41]K. K. Thornber (private communication).

[42]Yia-Chung Chang, D.Z.-Y. Ting, J. Y. Tang, and K. Hess, Appl. Phys. Lett. **42**, 76 (1983).

[43]The elementary formulation outlined here can be found in any textbook of quantum mechanics, such as, J. J. Sakurai, *Advanced Quantum Mechanics* (Addson-Wesley, Reading, 1973), p. 64. A more formal and general discussion of the correlation between decay of quasiexcitations and self-energy can be found in W. Heitler, *Quantum Theory of Radiation* (Clarendon, Oxford, 1970), Chap. IV, or J. M. Ziman, *Elements of Advanced Quantum Theory* (Cambridge University Press, Cambridge, 1969), Chap. 4.

[44]James H. Davenport, Patrizia Gianni, Richard D. Jenks, Victor S. Miller, Scott C. Morrison, Michael Rothstein, Christine J. Sundaresan, Robert S. Sutor, and Barry M. Trager (unpublished).

[45]Peter J. Price, Semicond. Semimet. **14**, 249 (1979).

[46]Carlo Jacoboni and Lino Reggiani, Rev. Mod. Phys. **55**, 645 (1983).

[47]T. Kurosawa, in *Proceedings of the International Conference on the Physics of Semiconductors, Kyoto* [J. Phys. Soc. Jpn. Suppl. A **49**, 345 (1966)]; H. D. Rees, Phys. Lett. A **26**, 416 (1968); J. Phys. Chem. Solids **30**, 643 (1969).

[48]N. Metropolis and S. Ulam, J. Am. Stat. Assoc. **44**, 335 (1949).

[49]J. von Neumann, in *Monte Carlo Method* Natl. Bur. of Stand. (U.S.) Spec. Publ. (No. 12, U.S. G.P.O., Washington, D.C., 1951), pp. 36–38.

[50]A simple monodimensional argument shows that the existence of a linear relationship between $\langle w \rangle$ and F is implied by a scattering rate increasing with energy as $w^{3/2}$, as in Eq. (11). Indeed, at steady state, the energy gained by an electron of velocity v from the field F must be equal to the energy lost to phonons of energy $\hbar\omega_P$ at a rate $1/\tau$; that is $evF=\hbar\omega_P/\tau$. Assuming simply $v=(2w/m^*)^{1/2}$, and expressing the linear dependence of w on F as $w=e\lambda F$, we obtain $1/\tau=evF/\hbar\omega_P=\text{const.}\times w^{3/2}$, which is the energy dependence of the nonpolar electron-phonon scattering rate at high energies as given by Eq. (11).

[51]See, for instance, K. Hess, Solid-State Electron. **21**, 123 (1978) and the discussions in Refs. 45 and 46 for examples related to transport in silicon. GaAs has been investigated, among others, by H. Shichijo, K. Hess, and G. E. Stillman, Appl. Phys. Lett. **38**, 80 (1981), and by H. Shichijo and K. Hess, Phys. Rev. B **23**, 4197 (1981).

[52]J. B. Socha, Ph.D. thesis, Cornell University, 1985.

[53]F. J. Himpsel, Th. Fauster, and D. Straub, J. Lumin. **31-32**, 920 (1984).

[54]The polaron-corrected electron effective mass m^*_{pol} is given by perturbation theory as $m^*_{\text{pol}}=m^*/(1-\alpha/6)$, where the parameter α is

$$\alpha=\frac{e^2}{8\pi\hbar\omega_{\text{LO}}}\left[\frac{2m^*\omega_{\text{LO}}}{\hbar}\right]^{1/2}\left[\frac{1}{\epsilon_>}-\frac{1}{\epsilon_<}\right]$$

and m^* is the electron effective mass in absence of the polar interaction with the optical phonons. In the case of SiO_2, the parameter α is about 1.35, considering only the 0.153 eV phonon. At low energies, where the polar interaction is dominant, we expect that $m^*\simeq 0.5 m_{\text{free}}$. Thus we should have $m^*_{\text{pol}}\simeq 0.64 m_{\text{free}}$. Good agreement between theory and the low-field mobility data can be obtained only with $m^*\simeq m_{\text{free}}$,

or by employing rather strong deformation potentials for the interaction between the electrons and the acoustic and (transverse) optical phonons. This has been done by H. Köster, Jr. and K. Hübner, Phys. Status Solidi B **118**, 293 (1983) with the choice of 3 eV and 2×10^9 eV/cm for the acoustic and optical deformation potential, respectively, and by W. Porod and D. K. Ferry, Phys. Rev. Lett. **54**, 1189 (1985), who chose the values of 25 eV for the acoustic intravalley and of 10^9 eV/cm for the intervalley deformation potential.

[55]A. Hartstein, Z. A. Weinberg, and D. J. DiMaria, Phys. Rev. B **25**, 7174 (1982).

[56]J. Y. Tang and Karl Hess, J. Appl. Phys. **54**, 5145 (1983).

[57]K. K. Thornber, Solid-State Electron. **21**, 259 (1978) and references therein.